Quantifying Global Cyclone Losses with Asset-Level Exposure and Dynamic Production Networks

Ruben Haalebos[1] and Peter Tankov[2]

[1]CREST, ENSAE, Institut Polytechnique de Paris, Électricité de France (EDF)
[2]CREST, ENSAE, Institut Polytechnique de Paris

February 28, 2026

Abstract

Tropical cyclones are a major source of climate-related losses, destroying capital and disrupting production. Global assessments often treat bottom-up damage estimation and macroeconomic impacts separately, limiting our ability to trace how asset-level damages translate into worldwide production and GDP losses. We develop a framework that combines (i) asset-resolved TC direct damages from exposure data and simulated TC tracks with (ii) an agent-based model that propagates shocks through inter-industry linkages. Losses are measured relative to a stable counterfactual baseline, enabling a decomposition into direct and indirect effects. Under SSP5–8.5, expected global direct damages remain modest but approximately double in the long term, while tail risk increases sharply: a historical 1,000-year loss level becomes a $\sim$200-year event in the near term and a $\sim$20-year event by 2075–2100. Production losses shift upward similarly, and indirect losses account for more than half of total production losses on average, with strong sectoral and regional heterogeneity. Network propagation amplifies impacts in exposed regions and generates material spillovers, so similar aggregate damages can produce very different GDP outcomes depending on the sectoral-geographic pattern of impacts. These findings have direct implications for the design of adaptation measures and for estimating climate-related financial risk.

1 Introduction

Tropical cyclones (TCs) are among the most destructive climate-related physical hazards. A recent report by Allianz estimates that, globally, TC-related events generate on the order of USD 78 million in economic damages per day Krichene et al. (2024). Beyond the destruction of capital, cyclones can disrupt production, logistics, and trade, with effects that propagate well beyond directly exposed areas Hallegatte (2008). Importantly, while the frequency of TCs is expected to remain broadly stable or even slightly decline, their intensity and associated rainfall are projected to increase under global warming, implying a rising potential for severe economic losses Seneviratne et al. (2021). Quantifying these impacts remains challenging for two reasons. First, translating hazard into damages requires detailed information on exposure and vulnerability at spatial and asset resolution, as aggregate statistics can mask substantial heterogeneity across sectors and locations Cardona et al. (2012); Simpson et al. (2021). Second, the economic costs of a TC event are not confined to direct physical damages: production networks can transmit shocks through intermediate-input bottlenecks, supplier failures, and demand contractions, generating indirect losses that may exceed the initial destruction and affect regions with little or no direct hazard exposure Hallegatte (2008); Kuhla et al. (2023). These propagation mechanisms create the possibility of nonlinear and state-dependent outcomes, in which similar aggregate direct damages translate into very different macroeconomic losses depending on which sectors are hit and on their centrality in supply chains Carvalho et al. (2021).

A growing literature documents such propagation dynamics, but it remains largely regional specific (e.g., national supply-chain disruptions following major disasters) Inoue and Todo (2019); Bressan et al. (2024). By contrast, global assessments of cyclone risk often fall into two complementary strands. A first strand focuses on quantifying direct physical damages using catastrophe-risk or impact-modeling approaches to produce loss metrics and return-period curves Gettelman et al. (2018); Le Guenedal et al. (2022); Meiler et al. (2022). A second strand studies the macroeconomic consequences of cyclones using country-level exposure indices, aggregate disaster measures, or reduced-form specifications to estimate effects on GDP and its components (Hsiang and Jina (2014); Mohan et al. (2018)), and more recently through macro-structural or general-equilibrium frameworks (Lehtomaa and Renoir (2023)). While highly informative, these strands are often developed with different levels of granularity and different representations of economic interdependence. In particular, global direct-damage assessments typically do not focus on damage propagation, whereas macroeconomic analyses frequently rely on shocks that are spatially and sectorally aggregated relative to asset-level exposure. This motivates an integrated framework that jointly combines (i) bottom-up, asset-resolved direct damages with (ii) their dynamic transmission through inter-industry and international trade linkages.

In this paper, we develop an integrated framework to produce bottom-up estimates of global TC direct physical damages, using open-source data. We then translate these damages into macroeconomic production losses using a dynamic Input-Output (IO) model that explicitly represents supply-chain interdependencies and supply- and demand-side disruptions. The direct-damage module combines asset-level exposure data with simulated TC tracks to generate asset-level damage fractions, which are then aggregated to sector-region units (hereafter, "industries"). The economic module is an agent-based model (ABM) with an explicit production network calibrated on Multi-Regional Input-Output (MRIO) data, yielding a consistent representation of global supply-chain linkages. Industry-level direct damages enter the model as exogenous climate shocks that reduce productive capacity. We then simulate the evolution of production and GDP over the year following the TC linked shocks. Following Hallegatte and Przyluski (2010), we measure losses relative to a counterfactual stable baseline, thereby quantifying the overall economic impact. This framework also allows us to decompose total losses into direct effects and indirect, network-induced propagation effects.

We apply this framework to study the economic effects of TC damages under an SSP5–8.5 scenario. We find that, while global direct damages remain modest in absolute terms, they are projected to approximately double between the historical period (1990-2015) and the long-term period (2075-2100). The upper tail also intensifies markedly: an event associated with a 1,000-year return period in the historical baseline becomes comparable to a $\sim$200-year event in the near term (2025–2050) and to a $\sim$20-year event in the long term. Consistent upward shifts are observed for production losses. Indirect losses transmitted through supply chains account for more than half of total production losses on average, with substantial heterogeneity across sectors and regions. This network channel both amplifies losses in directly exposed regions and generates material spillovers in regions with limited or no direct cyclone exposure, particularly for economies that are central to global supply chains. As a result, similar aggregate damage levels can translate into very different macroeconomic outcomes depending on the location and sectoral composition of impacts, giving rise to pronounced tail risks for specific industries.

Our results highlight the importance of accounting for propagation effects in production networks when studying the impact of TCs on the economy. Network transmission can generate nonlinearities in aggregate economic damages, with large shifts in effective exposure across sectors—both in directly affected regions and in regions with little or no physical exposure. The initial geographic and sectoral composition of the shock therefore matters, highlighting the value of targeted adaptation measures in economically central sectors and bottleneck industries. These mechanisms are also central for assessing climate-related financial risk: supply-chain propagation can amplify firm-level revenue losses and transmit shocks to upstream suppliers and downstream customers that are not directly hit by the hazard. The remainder of the paper is organized as follows. The next paragraph reviews the related literature. Section 2 presents the methodology. Section 3 reports the baseline results, and Section 4 examines nonlinear GDP responses and amplification effects, as well as a potential application to climate-related financial risk. Section 5 concludes.

Literature review A growing body of work documents the broad consequences of TCs across welfare, ecosystems, and the built environment. Recent contributions quantify the social costs of TCs Krichene et al. (2023), document ecosystem damages associated with intensifying cyclone activity Feehan et al. (2024), and study impacts on urban systems and infrastructure Shughrue et al. (2020). Together, these studies emphasize that cyclone risk extends beyond insured asset losses and can generate persistent societal and environmental consequences.

In parallel, the economics literature has examined how cyclones affect output and growth. Reduced-form and panel-based approaches use observed cyclone exposure and disaster measures to estimate impacts on GDP and its components, often highlighting persistent effects Hsiang and Jina (2014); Mohan et al. (2018). Complementary event-based analyses and accounting approaches document that indirect and higher-order losses can be quantitatively important relative to direct damages, especially when disruptions propagate through production linkages Lenzen et al. (2019); Kunze (2020). More recently, macro-structural and general-equilibrium perspectives have been used to interpret the incidence of cyclone shocks through sectoral reallocation and price mechanisms Lehtomaa and Renoir (2023). Overall, this evidence motivates modelling approaches that connect the spatial and sectoral footprint of physical shocks to macroeconomic outcomes through propagation channels.

A third strand focuses on forward-looking assessments of cyclone damages under climate change. Impact-modelling platforms such as CLIMADA Aznar-Siguan and Bresch (2019) facilitate globally consistent, bottom-up risk assessments that combine hazard, exposure, and vulnerability modules, and have enabled applications at increasingly granular scales, including asset- and firm-level risk analysis Bressan et al. (2024). Related work estimates how direct cyclone damages may evolve across warming scenarios using high-resolution climate information and synthetic event sets Gettelman et al. (2018); Le Guenedal et al. (2022); Meiler et al. (2022). More broadly, recent MRIO-based evidence highlights that indirect losses from extreme events can be of similar magnitude to direct losses and may be substantially amplified through international trade linkages Wang et al. (2025).

Measuring the indirect economic costs of disasters is central for risk management and policy design Hallegatte (2014). A common modelling route represents the economy as a production network—often calibrated on MRIO tables-and simulates adjustment dynamics following shocks. The ARIO model pioneered by Hallegatte (2008) illustrates how disaster-induced capacity constraints can generate indirect losses through supply bottlenecks and demand spillovers. Related global agent-based production-network frameworks such as *Acclimate* illustrate how local disruptions can cascade internationally and generate indirect losses comparable to direct ones Otto et al. (2017). Complementary approaches propose network metrics to identify bottlenecks and assess the potential for cascading production shortages, including the Production Shortage Interdependence (PSI) measure developed by Glanemann et al. (2016). Related agent-based or network-based frameworks have been applied to other large disruptions, such as COVID-19 lockdown shocks Pichler et al. (2022), and to the study of resilience and out-of-equilibrium dynamics in production networks Klimek et al. (2019); Dessertaine et al. (2022). At the micro level, similar tools have been used to quantify shock propagation in firm-to-firm networks Inoue and Todo (2019), and extensions incorporate transport and logistical constraints as additional propagation channels Colon et al. (2021).

Recent policy-facing applications also emphasize the macro-financial relevance of cross-border propagation: the ECB Working Paper by Fahr et al. (2024) shows how physical-risk shocks can be amplified through IO linkages, with implications for stress testing and the mapping from real-economy disruptions to financial risk. Building on these strands, our contribution is to combine bottom-up, asset-resolved estimates of TC direct damages with a dynamic production-network model calibrated on MRIO data, enabling a globally consistent mapping from physical impacts to direct and indirect economic losses through cross-border supply-chain linkages.

2 Methods

2.1 Estimation of the geographic distribution of production

We estimate the geographic distribution of production across sectors by combining asset-level data from ClimateTRACE with sectoral output from the GLORIA (Global Resource Input-Output Assessment) MRIO database. MRIO tables describe interlinkages between sectors and regions at the global scale; throughout the paper, we refer to a sector–region pair as an "industry". The MRIO framework reports intermediate input flows between industries in monetary terms (see Appendix 6.1 for a more detailed presentation on the structure of these tables). This integration enables us to estimate industry-level climate risk while accounting for the spatial distribution of production sites. As a result, our results are region-specific and depend on the within-region geographic allocation of sectoral activity. Implementing the merge requires, first, a concordance between the regional and sectoral classifications used in ClimateTRACE and GLORIA [1]. We aggregate countries into 22 regions, distinguishing cyclone-prone areas from non-exposed areas, and we consider 44 sectors. For a subset of sectors, asset-location information is unavailable; these sectors are therefore assumed to be exposed only through indirect losses. The full procedure used to construct the dataset is described in Appendix 7.1.

As a result, we obtain set of assets $\mathcal{A}$ of size N, with $\mathcal{A} = \{a_1, \ldots, a_N\}$. Each element a_l is composed of a position $P_l^{\text{asset}} = \{\text{lat}_l, \text{lon}_l\}$, a size (capacity) K_l^{asset} and a production x_l^{asset}, both expressed in monetary values. For each industry i, the sum of asset-level capacities and productions equals the corresponding industry-level totals. Each asset is assigned to a unique industry, and we define the mapping $I(.)$ (resp. $R(.)$ and $S(.)$) that returns the industry (resp. the region and the sector) associated with a given asset, i.e., $I(a_\ell) = i$

2.2 Tropical cyclone modelling

Wind speed data from tropical cyclone is generated using the Cyclone generation Algorithm including a THERmodynamic module for Integrated National damage Assessment (CATHERINA) model. This model couples statistical and thermodynamic relationships to generate synthetic cyclone tracks sensitive to local climate conditions and estimates the damage induced

[1] Details on the mapping can be provided upon request.

by tropical cyclones. The framework is compatible with the data from CMIP (Coupled Model Intercomparison Project) models offering a reliable solution to resolve tropical cyclones in climate projections. In Appendix 6.2, we illustrate the generation process of tropical cyclones, and we refer to Le Guenedal et al. (2022) for a full description of the model. Using this framework, we construct a database of synthetic tropical cyclones for two distinct periods:

- Historical simulations: 1990–2015.
- Forecasted simulations, subdivided into three time slices:
  - Near-term: 2025–2050,
  - Mid-term: 2050–2075,
  - Long-term: 2075–2100.

Simulations over the historical period allow us to benchmark the model by comparing wind speed with those of the International Best Track Archive for Climate Stewardship (IBTrACS) dataset Knapp et al. (2010). For each period, we run $n_{\text{sim}} = 100$ simulations, yielding a total of 2,500 simulated (representative) years across all time slices. We use the ACCESS-CM2 climate model Dix et al. (2019) under the SSP5-8.5 scenario to provide the climate variables required by the intensification module [2].

A cyclone (observed or simulated) is described by the evolution of a wind speed denoted by v (measured in $m.s^{-1}$) at different latitudes and longitudes between a starting time t_0 and a final time t_T. We call $P_{t,k}^{\text{cyclone}} = (\text{lat}_{t,k}, \text{lon}_{t,k})$ the position of cyclone k at time t. A tropical cyclone k can thus be defined by a track T_k that represents the evolution of the wind of the cyclone at different positions, with :

$$T_k = \{(v_{t,k}, P_{t,k}^{\text{cyclone}})\}_{t=t_0}^{t_T}$$

2.3 Industry-level damage fraction estimation

We first compute asset-level damage fractions for both observed and simulated tropical cyclones. The complete methodology is described in Appendix 7.2. We use the wind-damage function of Emanuel (2011):

$$f(v, v_h^r) = \frac{\max(v - v_0, 0)^3}{(v_h^r - v_0)^3 + \max(v - v_0, 0)^3} \tag{1}$$

Equation 1 maps an observed wind speed v to an asset-level damage fraction. We set the threshold parameter $v_0 = 92.5\,\text{km}\,\text{h}^{-1}$, which corresponds to the minimum wind speed at which damages occur. The parameter v_h^r is region specific and calibrated following the work of Eberenz et al. (2021). We apply the same damage function across all industries and periods, thereby abstracting from sector-specific adaptation and mitigation measures. Estimating industry-specific vulnerability parameters, as well as the potential impact of adaption measures on the damage curve is left for future work.

We compute the wind speed v used to derive each asset's damage fraction as follows. For each cyclone, we check whether its track passes within 200 km of the asset location; if so, we select the associated wind speed used in the damage calculation for that asset. This wind speed is selected as follows:

- Observed cyclones: we use the maximum wind speed reported along the observed track within the 200 km radius,

[2] We are currently expanding the analysis to include additional climate models and emissions scenarios.

- Simulated cyclones: we use the q-th quantile of distribution of wind speeds within the 200 km neighbourhood.

The quantile q is calibrated at the regional level by minimizing, over the 1990–2015 period and across all assets in the region, the discrepancy between damages computed from observed cyclones and those computed from simulated cyclones. The selected wind speed associated to asset l from cyclone k is $\tilde{v}_{k,l}$.

The damage fraction experienced by asset ℓ due to cyclone k is

$$\epsilon_{k\ell} = f\left(\tilde{v}_{k\ell},\, v_h^{R(\ell)}\right), \tag{2}$$

We then define the industry-level damage fraction in year y as a capacity-weighted average of asset-level damages, where each asset is assigned the maximum damage it experiences across all cyclones occurring in year y:

$$\zeta_i(y) = \frac{\sum_{\ell \in \mathcal{A}_i} \left(\max_{k \in \mathcal{TC}_y} \epsilon_{k\ell}\right) K_\ell^{\text{asset}}}{\sum_{\ell \in \mathcal{A}_i} K_\ell^{\text{asset}}}. \tag{3}$$

Here, $\mathcal{A}_i$ denotes the set of assets belonging to industry i, and $\mathcal{TC}_y$ the set of cyclones occurring in year y. The industry-level damage fraction $\zeta_i(y)$ is then used as an input to the production network model to parametrize tropical-cyclone-induced shocks. Following Aznar-Siguan and Bresch (2019), we define the expected annual impact (EAI) for industry i as the expected value of its annual loss, thus capturing both event frequency and loss severity:

$$\text{EAI}_i \;=\; \mathbb{E}[\zeta_i(y)]\,,$$

where $\zeta_i(y)$ denotes the annual loss experienced by industry i in year y. In practice, we compute the empirical mean of EAI_i over a 25-year window $\mathcal{Y}$ as

$$\widehat{\text{EAI}}_i \;=\; \frac{1}{|\mathcal{Y}|} \sum_{y \in \mathcal{Y}} \zeta_i(y)$$

2.4 Production network model

We use a production network model calibrated on the GLORIA MRIO database, which provides a realistic representation of inter-industry linkages. Following Dessertaine et al. (2022), the model is composed of three main epochs, illustrated in Figure 1, and is adapted to account for damages and reconstruction dynamics in the spirit of Hallegatte (2008) and Juhel (2024).

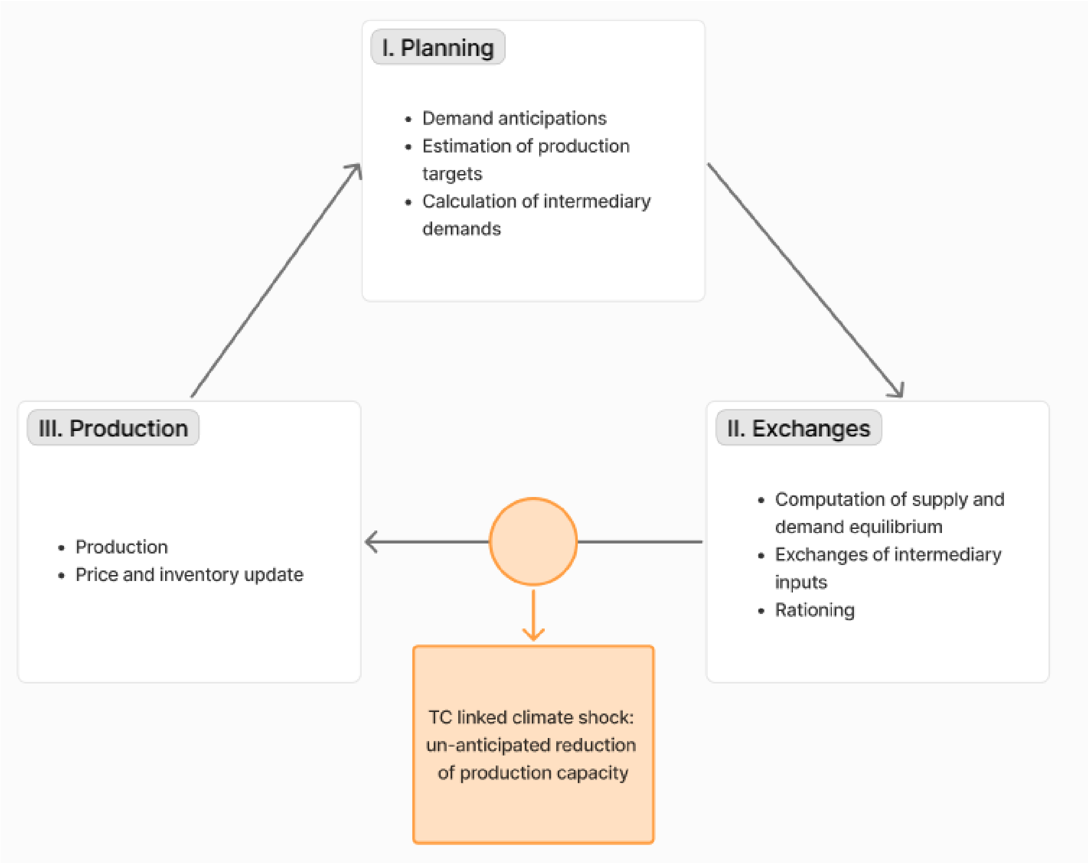

Figure 1: Illustration of the three main epochs of the production network model.

A complete description of the model is provided in Appendix 8. Below, we briefly summarize the key mechanisms and provide intuition for the main channels at work.

The model features $M = 22 \times 44 = 968$ industries and $N = 22$ representative households. Each industry produces a single good using intermediate inputs, sourced from other industries, and labour. Households supply labour and consume goods produced by industries. Inter-industry linkages are described by the production network, represented by the matrix of technical coefficients derived from the MRIO table. The model is simulated at a monthly frequency, indexed by $t \in \{0, 1, 2, \dots\}$.

At the beginning of each monthly step, baseline supplies and corresponding prices are known. The dynamics then proceed in three steps. In the first stage (planning), industries form expectations about intermediate demand from other industries and final demand from households, and use these expectations to set a planned level of production. Planned production in turn determines desired intermediate input purchases and labour demand. In the second stage (exchange), households supply labour and goods are traded. Whenever demand for an industry's output exceeds its available supply, a rationing mechanism is applied. In addition, we allow for transport-related rationing for trade-intensive sectors: trade flows are constrained when transport infrastructure in either the exporting or the importing industry is affected by a TC shock. Between the exchange and production stages, an unanticipated climate shock may occur. As defined in equation 4, a TC shock reduces the effective production capacity of affected industries, so that realized output may fall short of planned output, potentially generating imbalances in the next period. In the final stage (production), each industry produces subject to demand, the availability of intermediate inputs and labour, and its effective production capacity. After production takes place, prices are updated and adjust to observed supply and demand imbalances.

Reconstruction of damaged productive capacity begins in the period immediately following the TC shock. Recovery follows a concave rebuilding function, and reconstruction activity generates additional demand directed toward the local construction industry.

Cyclone damages are calibrated on for representative years. For each year y in a given period (historical or future) we compute an industry-level damage fraction vector

$$\boldsymbol{\zeta}(y) = \big(\zeta_1(y), \ldots, \zeta_M(y)\big),$$

which summarizes the TC-induced capacity loss for all industries. We implement the TC shock as a proportional reduction in productive capital that applies at the shock month t_τ. Specifically, the maximum feasible output of industry i at t_τ satisfies

$$x_i(t_\tau) \;\leq\; \big(1 - \zeta_i(y)\big)\, \nu_i\, K_i(t_\tau) \;=\; \big(1 - \zeta_i(y)\big)\, x_i^K(t_\tau), \tag{4}$$

where ν_i is the capital-to-output conversion rate and $x_i^K(t) \equiv \nu_i K_i(t)$ denotes the capacity-implied upper bound on production. We assume ν_i is time-invariant and initialize it from the baseline steady state as $\nu_i = x_i(0)/K_i(0)$. This specification abstracts from post-disaster adaptation (e.g., resilience investments, changes in production processes, or improved protection standards) that could alter ν_i over time; incorporating endogenous adaptation is left for future work.

A single run of the economic model corresponds to selecting one representative year y (and, in simulated periods, one Monte Carlo draw), and injecting the corresponding representative-year shock vector $\boldsymbol{\zeta}(y)$ into the monthly model. Importantly, the shocks for *all* industries enter the model simultaneously (i.e., as a single economy-wide shock vector)[3], while the economic adjustment and reconstruction dynamics unfold at the monthly time scale t.

Formally, letting t denote the monthly index and y the (representative) shock year used to parameterize a given run, the model dynamics can be written as

$$\mathbf{x}(t+1),\, \mathbf{p}(t+1),\, \mathbf{K}(t+1) = \mathcal{M}\left(\mathbf{x}(t),\, \mathbf{p}(t),\, \mathbf{K}(t),\, \boldsymbol{\zeta}(y)\right), \tag{5}$$

where $\mathbf{x}(t)$ denotes the vector of industry-level production, $\mathbf{p}(t)$ the vector of prices, and $\mathbf{K}(t)$ the vector of effective production capacities at month t. The mapping $\mathcal{M}(\cdot)$ summarizes behavioural rules, market-clearing and rationing mechanisms, and reconstruction dynamics.

2.5 Direct, indirect and GDP damages computation

The economic model is simulated at a monthly frequency. Cyclone impacts on production are measured as the deviation from a counterfactual baseline trajectory without shocks, i.e., as the difference between the shocked and baseline outcomes. We consider a simple baseline outcome where not event occur, following Hallegatte and Przyluski (2010), but more complex baseline including chronic shocks a in Bressan et al. (2024) could be implemented. In our specification, we impose a single climate shock that affects all industries simultaneously. This assumption is consistent with our construction of annual industry-level damages, which uses the maximum cyclone impact within a year.[4]. We define the following indicators for production and Gross

[3] A more realistic approach would account for region-specific cyclone seasons and the resulting staggered timing of shocks across regions. Incorporating such seasonality would increase the modelling complexity, and we therefore adopt the parsimonious specification in the present version. As a consequence, our estimates—in particular for indirect losses—may be biased upward.

[4] A more realistic approach would account for region-specific cyclone seasons and the resulting staggered timing of shocks across regions. Incorporating such seasonality would increase modelling complexity, and we therefore adopt the parsimonious specification in the present version. As a consequence, our estimates–in particular for indirect losses–may be biased upward.

Domestic Product (GDP [5]) loss:

$$
\begin{aligned}
\mathcal{L}_i^{total} &= \sum_{t=t_0}^{t_0+12} (x_i(t) - x_i(t_0)) \\
\mathcal{L}_i^{direct} &= \sum_{t=t_0}^{t_0+12} (x_i^K(t) - x_i^K(t_0)) \\
\mathcal{L}_i^{indirect} &= \mathcal{L}_i^{total} - \mathcal{L}_i^{direct} \\
\mathcal{L}_i^{GDP} &= \sum_{t=t_0}^{t_0+12} (\mathrm{GDP}_i(t) - \mathrm{GDP}_i(t_0))
\end{aligned}
\tag{6}
$$

Losses are expressed in monetary units. We also report normalized loss ratios defined relative to annual baseline production:

$$l_i^{\text{total}} = \frac{\mathcal{L}_i^{\text{total}}}{12\, x_i(t_0)},$$

with analogous definitions for direct and indirect losses, l_i^{direct} and l_i^{indirect}. Normalized GDP loss ratio is defined relative to the GDP baseline.

3 Results

In this section, we present and interpret the model outcomes under the SSP5–8.5 scenario, using the ACCESS-CM2 climate model to simulate tropical cyclone. We focus on SSP5–8.5 because it represents a high-emissions, high-warming pathway, and therefore provides a deliberately stress-tested setting in which climate-change-driven shifts in cyclone intensity and associated economic damages are most pronounced. The analysis proceeds in two steps. First, for each of the four 25-year periods considered, we compute industry-level damage fractions. Second, these damage fractions are introduced as shocks into the economic model, from which we derive direct losses, indirect losses, and associated GDP losses at both the sectoral and regional levels. For each 25-year period, we run 100 Monte Carlo simulations. This yields 2,500 simulation–year observations per period for each of the 968 industries, resulting in a large panel of loss outcomes across periods, simulations and industries. The objective of this section is to highlight the main patterns and robust findings emerging from this dataset. While the framework naturally supports more granular industry-specific case studies, we leave such disaggregated analyses to future work.

3.1 Bottom-up estimation of TCs linked direct damages

The first step of our framework delivers global bottom-up quantification of direct damages from tropical cyclones. As shown in Figure 2a, aggregate impacts remain modest at the global scale. In the observed record, the industry-weighted EAD at global level corresponds to roughly 0.1% of global productive capacity destroyed; under the long-term period, this average is projected to approximately double. Estimated damages for the simulated historical period are somewhat higher than their observed counterparts. This difference reflects our the Monte Carlo design: with 100 simulations, rare but very large loss realizations can occur in the pooled sample, mechanically raising the sample mean.[6] The increase in risk is more pronounced when focusing

[5] The GDP is a direct output from the economic model, and computed as total production net of intermediate input use.

[6] Appendix 7.3 reports the same comparison using the median annual damage ratio by industry. At that level, simulated and observed historical damages are broadly consistent, suggesting that the difference in means is driven by the upper tail rather than by a systematic shift of the central tendency.

on extremes. Figure 2 reports return levels of global industry-weighted EAD as a function of the return period. We observe a the strong leftward shift of the tail: an event with a 1,000-year return period in historical sample becomes comparable to a ∼200-year event in the near-term, and to an event occurring on the order of ∼20 years in the long-term. This compression of return periods indicates a substantial rise in the frequency of high-damage events, with potentially large implications for capital destruction and economic disruption.

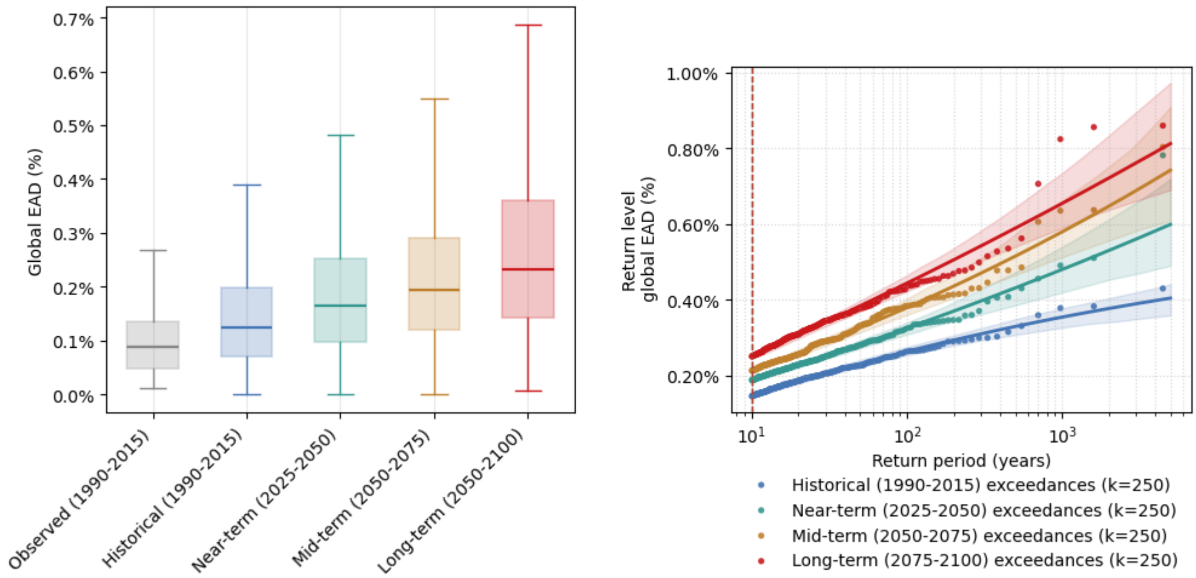

(a) Evolution of the global industry-weighted EAD.

(b) Evolution of extreme realisations of global industry-weighted EAD. Note: Excedancees are selected as realisation above the 90th quantiles.

Figure 2: The global industry-weighted EAD is projected to increase over time, both in average and extreme-loss outcomes.

These estimates should be interpreted in light of model limitations. In particular, the damage calculations are conditional on fixed exposure and vulnerability and therefore do not incorporate endogenous adaptation, protective investments, or the relocation of productive capacity. Nevertheless, the results highlight a material intensification of cyclone-related tail risk. They underscore the necessity of mitigation to limit further warming, as well as the need to accelerate adaptation planning, especially given that near-term climate conditions are largely locked in by past and current emissions.

3.2 Indirect production losses account for more than half of total losses

Next, we examine the economic consequences of these direct capacity shocks. We begin by constructing normalized indicators of direct and indirect production-loss ratios. Figure 3 reports the decomposition of global production losses into their direct and indirect components. For each simulation-year, we aggregate direct (resp. indirect) production losses across all industries, and normalize by total baseline production to obtain a global loss ratio. We then average these ratios over years within each period. The dispersion bands in the figure reflect simulation variability. At the global level, production losses remain small: the mean loss ratio is approximately 0.015% in the historical period and increases to nearly twice that level in the long-term period. These values are notably smaller than the corresponding capacity-destruction ratios, which is expected because production losses are measured relative to an annual baseline and therefore capture the flow impact over the year. A key result is that indirect losses account for a substantial share of total production losses. Globally, the indirect component represents more than half of aggregate losses, indicating that network propagation mechanisms—through supply shortages, input bottlenecks, and demand spillovers—are quantitatively at least as important as the initial, localized destruction of productive capacity. This finding highlights the relevance of explicitly modelling production networks: neglecting indirect effects would omit a large fraction of total impacts and understate the economic cost of cyclone-induced disruptions.

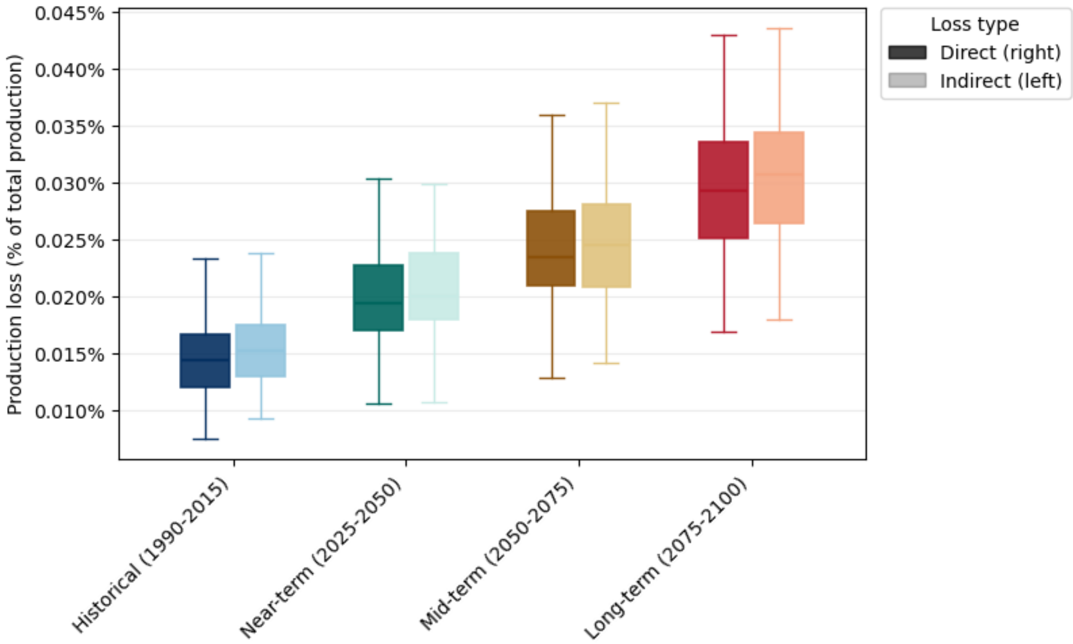

Figure 3: Total production loss decomposed into direct and indirect components, aggregated across regions and sectors. Note: For each simulation, direct and indirect losses are computed as the median over the 25-year horizon (one point per simulation).

There is, of course, substantial heterogeneity across sectors and regions. Figure 4 summarizes this dispersion by reporting, for each period, the average impact computed across all simulations and years for the 10 most affected regions and the 15 most affected sectors. The figure reveals a set of highly exposed regions: Japan, Southeast Asian islands, China, and the United States. Within these regions, some sectors exhibit persistently high exposure across locations—notably chemicals, energy, and electricity generation and distribution—reflecting both their direct vulnerability. Other sectors display more heterogeneous patterns: for instance, steel-related industries can be primarily directly affected in some regions, yet more indirectly affected in others, depending on the geographic location of productive assets and the region's position within global supply chains. Finally, the figure also highlights that sizeable impacts can arise in regions with no direct cyclone exposure. Western Europe, for example, experiences non-negligible losses despite no direct damages, with the entire effect operating through network propagation. This underscores that exposure is not purely geographic: even regions outside cyclone-prone areas can face material economic losses through production-network interdependencies.

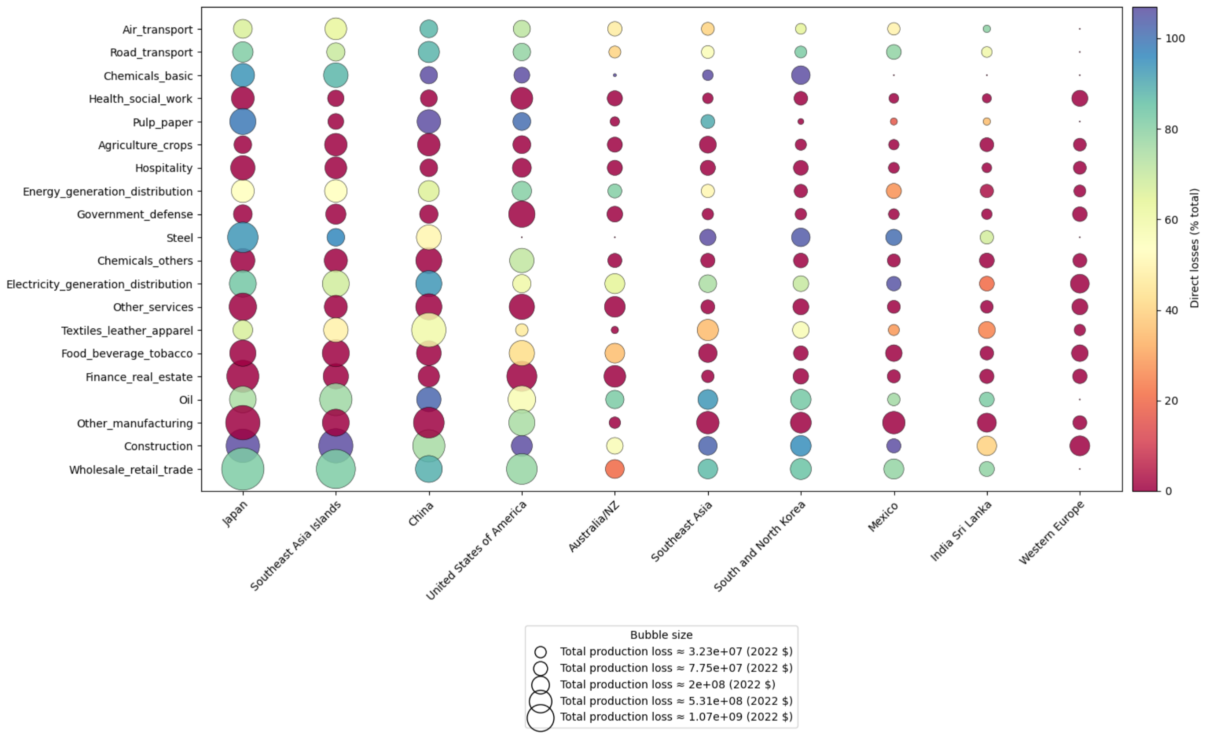

Figure 4: Regional and sectoral production losses, for the Near-term period (2025-2050). Note: The results are averaged over all simulations. The bubble size indicates the size of the output loss while the colour indicates the proportion of output loss due to direct losses.

3.3 Supply-chain linkages transmit the damages to unaffected regions

To jointly capture direct and network effects, we next consider impacts on GDP. In our MRIO setting, we measure GDP as value added, defined as total gross output net of intermediate input use. This metric reflects both direct and indirect production losses, while also allowing for positive effects from additional activity induced by reconstruction demand.

Figure 5 presents the regional distribution of GDP losses. The bubble colour indicates the share of direct production losses in total production losses. Thus, it provides a compact summary of whether local destruction or network propagation is the dominant transmission channel. Three broad regional profiles emerge. First, highly exposed regions combine sizeable losses with a relatively balanced decomposition between direct and indirect components (e.g., Japan and Southeast Asian islands). Second, several regions experience large GDP losses despite a predominance of indirect effects, indicating that their losses are driven mainly by supply-chain amplification of local asset destruction (notably the United States, China, Southeast Asia, Australia, and Mexico). Third, regions with no direct cyclone exposure nonetheless exhibit important GDP losses that are entirely indirect (e.g., Europe, South America, and Russia).

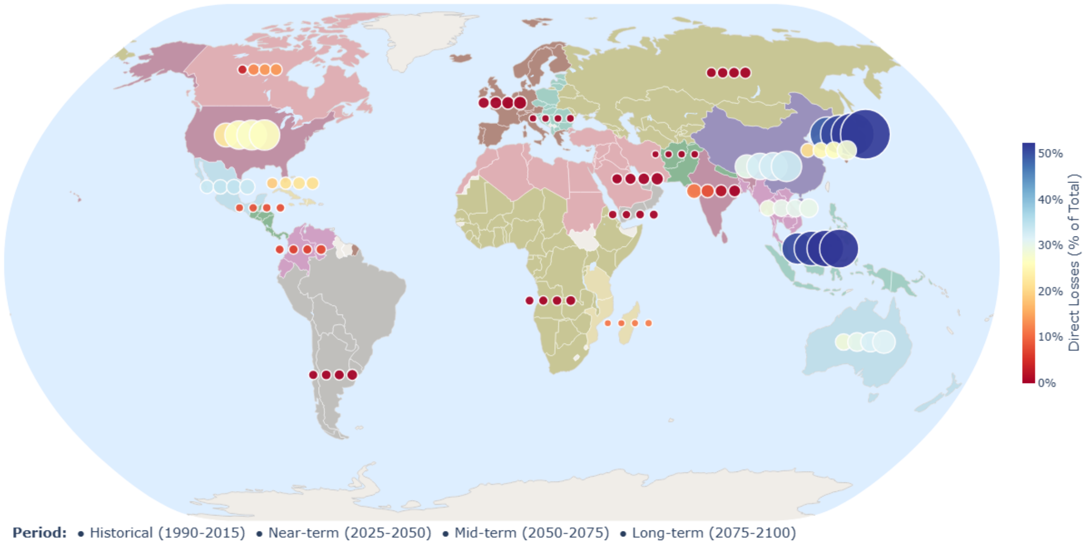

Figure 5: GDP loss by country, for the four different periods. Note: the bubble colour indicates the share of total production losses attributable to direct losses.

Overall, the figures in this section underscore that production-network linkages are a key determinant of the spatial distribution of aggregate losses. The results reported above, however, primarily describe average outcomes across simulations and years. In the next section, building on empirical evidence that shocks can propagate and be amplified along upstream and downstream supply-chain relationships, we illustrate how production networks can generate substantial amplification effects and reveal hidden exposures that are not visible from local hazard intensity alone Carvalho et al. (2021). This perspective is particularly relevant for financial physical-risk assessment: firms with limited or no direct exposure to the hazard may nonetheless experience material output and value-added losses through disruptions affecting critical suppliers, customers, or complementary inputs elsewhere in the network.

4 Discussion

4.1 Nonlinear GDP responses to TC induces damages

The results from the previous section exhibit high heterogeneity in exposure across sectors and regions. Consequently, cyclones associated with similar levels of aggregate direct damage can generate markedly different macroeconomic outcomes, depending on where the damages occur and which industries are hit. This point is illustrated in Figure 6, which plots, across all periods, simulations, and years, global GDP losses as a function of the return period of global direct damages. The figure suggests a positive association on average: larger direct-damage events (higher return periods) tend to coincide with larger GDP losses. However, this relationship is not strictly linear. A substantial number of observations lie well above the central trend. This indicates that for a given level of aggregate direct damage, GDP losses can be significantly amplified. These “outliers” reflect configurations in which the sectoral and regional distribution of damages interacts with the production network to generate disproportionate spillovers (for example through disruptions to highly central suppliers, bottlenecks in critical inputs, or cascading demand contractions). Quantitatively, this amplification can raise global GDP losses by as much as a factor of ~ 4 relative to outcomes associated with more “typical” damage allocations at comparable aggregate shock size.

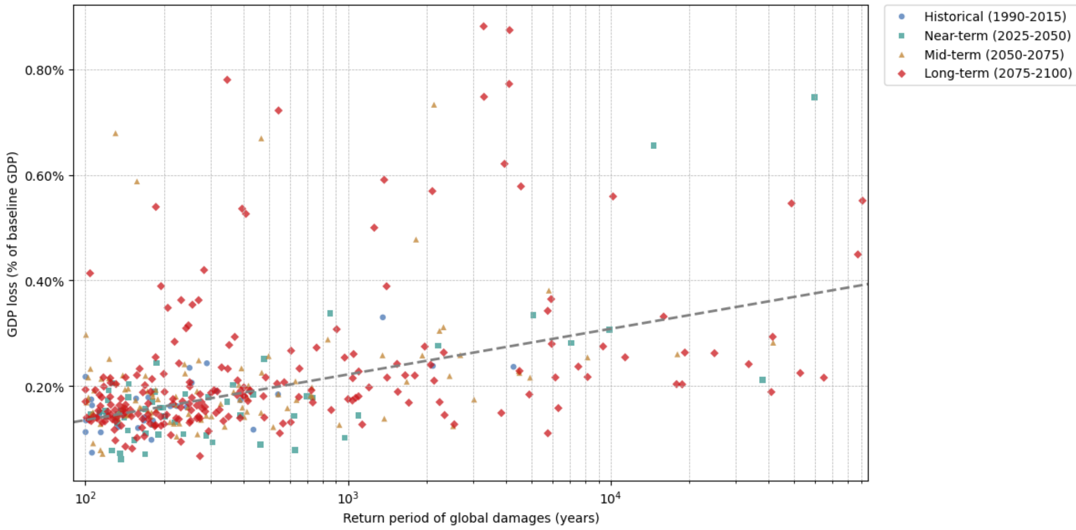

Figure 6: Global GDP loss as a function of direct damages return period. Note: one point represents the global GDP loss for a single simulation.

From a risk perspective, the cases in the upper-left corner are the most consequential: they correspond to realizations in which the GDP impact of an event is two to three times larger than the baseline impact expected for a shock of comparable aggregate direct damage. Most of these amplified realizations arise in the long-term period, consistent with the increasing severity and frequency of extreme cyclone-induced damages. Nevertheless, amplification effects are not confined to the far future: they already appear in the mid-term period and, in a few cases, can occur even in the near-term. This underscores that non-linear macroeconomic losses are not only a long-run concern, but a relevant feature of near- to medium-horizon risk under plausible climate trajectories.

4.2 Migration of mean and extreme losses between scenarios

To further characterize the sectoral and regional dimensions of this nonlinearity, we compare the distribution of losses across two subsets of events, defined by the magnitude of global direct capacity destruction. Specifically, we split the simulation-year observations into (i) "moderate" events, for which global direct damages are below 0.2%, and (ii) "extreme" events, for which global direct damages exceed 0.4%. The first subset corresponds to the range in which the GDP-loss/direct-damage relationship is, on average, close to linear, whereas the second subset isolates realizations in which amplification mechanisms are most likely to be active. For each subset, and for each region–sector pair, we compute two summary statistics of the resulting loss distribution: the mean and the 95$^{\text{th}}$ percentile. Figures 7a and 7b report these statistics for the United States and Western Europe, respectively. Importantly, the "extreme" subset is, by construction, rare: it aggregates low-frequency, high-severity realizations. As a result, the conditional tail outcomes reported for this subset should be interpreted as *losses conditional on an extreme global-damage state*, rather than as unconditional high-probability outcomes.

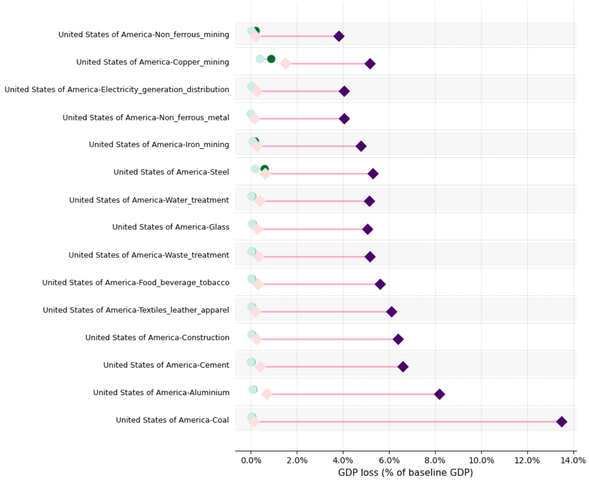

(a) Top 15 Sectors with Largest Shift in Extreme Losses (US).

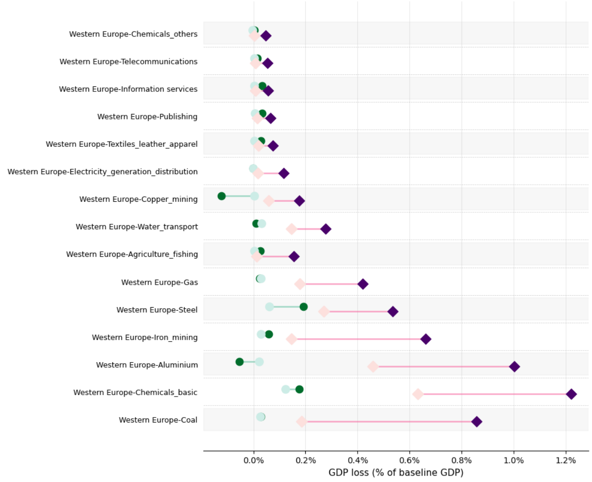

(b) Top 15 Sectors with Largest Shift in Extreme Losses (Western Europe).

Figure 7: Migration of Median and Extreme Losses Between Scenarios. Note: The green dot show the mean loss, while the purple dot show the 95th quantile loss. The shift is between case where global GDP loss is lower than

Figure 7a shows that differences in average losses between moderate and extreme events are relatively modest compared to the changes in the upper tail. In particular, the scale of variation in the 95^{th} percentile dominates the mean, indicating that a subset of sectors experiences a sharp thickening of the loss distribution under extreme global-damage realizations. In other words, amplification in the production network manifests less through a uniform upward shift of typical outcomes, and more through a disproportionate increase in the likelihood of very large sectoral losses. The contrast is particularly informative for Western Europe, where impacts are primarily indirect and arise almost entirely through production-network propagation (Figure 7b). As expected, the overall magnitude of losses is lower than in directly exposed regions. Nevertheless, the conditional tail can remain economically meaningful for specific upstream- or input-intensive industries, in which disruptions to key suppliers and intermediate goods propagate strongly. Finally, the figures also suggest that some sectors may exhibit small positive effects in average terms (e.g., copper mining or aluminium production), consistent with temporary demand reallocation and reconstruction-driven increases in activity when shortages elsewhere constrain supply. Such gains should be interpreted cautiously: they reflect short-run general-equilibrium rebalancing within the model rather than an absence of welfare losses from the underlying shock.

4.3 Implication for financial impact of climate change

In this study, we restrict attention to macroeconomic outcomes. However, the framework can be extended to quantify the implications of physical climate risks for financial risk. In particular, following the framework fromKerkhofs et al. (2025), the financial impact of tropical-cyclone (TC) events can be mapped into firm valuation through a discounted cash-flow (DCF) model, in which the value of a firm is determined by the present value of its expected future free cash flows (FCF). Using a standard DCF formulation, the value of firm f's asset ℓ can be written as

$$A_{f,\ell} = \sum_{t=0}^{T} \frac{FCF_t}{(1+r)^t} + TV,$$

where FCF_t denotes free cash flow at time t and r is the (constant) discount rate. The terminal value is given by the Gordon growth expression,

$$TV = \frac{FCF_{T+1}}{r - g},$$

where g is the long-run growth rate of free cash flows (with $r > g$).

TC-induced shocks can affect asset values through (at least) two channels. First, direct physical damages can destroy or impair productive capital. Second, production disruptions can depress revenues, raise input costs, and reduce operating margins even in the absence of local asset destruction. For clarity in this illustrative discussion, we abstract from insurance coverage. We note that our framework delivers direct estimates of both channels. The impact on capital is obtained from the asset-level damage fractions computed in the hazard–exposure module. The impact of production disruptions on operating performance is captured by the economic model, which produces industry-level profit (and output) responses to shocks (Appendix 8 provides details on the profit accounting).

More importantly, the illustrative application highlights the quantitative relevance of production-network propagation. Relative to direct effects alone, incorporating supply-chain spillovers can increase aggregate impacts. In our example, it approximately doubles the overall effect. In addition, network transmission generates indirect exposure: firms and sectors with no local physical damages can still experience significant losses through upstream input shortages, downstream demand contractions, or price and substitution effects. This underscores that assessments based solely on direct hazard exposure may materially understate both the magnitude and the breadth of climate-related financial risk.

5 Conclusion

In this work, we provide a bottom-up estimation of TC direct physical damages using asset-level exposure data and simulated TC hazard fields. We then study the transmission of these shocks through an ABM economic model, calibrated on MRIO data. Our results indicate that under a high-emissions pathway with increasing global greenhouse-gas (GHG) concentrations, expected global TC-related damages approximately double and extreme events become substantially more frequent. Moreover, indirect production losses arising from supply-chain disruptions account, on average, for more than half of total production losses. While cyclone-related damages are unsurprisingly concentrated in directly exposed regions, we also find non-negligible losses in regions with little or no direct hazard exposure when they are strongly connected to affected areas through trade and IO linkages. This highlights that vulnerability is shaped not only by local physical exposure, but also by a region's embeddedness in global production networks.

Our results also highlight production-network amplification. Events associated with similar levels of aggregate direct damage can generate markedly different GDP losses, depending on which regions and sectors are affected and on their position within global supply chains. In particular, certain damage configurations trigger disproportionate spillovers, implying that sectors typically viewed as weakly exposed can become highly vulnerable in specific network states. These findings are directly relevant for assessing financial risk from physical hazards: (i) production-network propagation can amplify revenue losses beyond the initial direct shock, and (ii) firms and sectors with no direct hazard exposure may nonetheless experience material revenue declines due to upstream or downstream disruptions.

The present analysis is intentionally narrow in scope, focusing exclusively on TC. As climate change progresses, other classes of physical risks - including riverine and pluvial floods, droughts, and heat extremes - are expected to intensify and to affect a broader set of geographies and sectors. The joint realization of multiple hazards, potentially correlated in time and space, could amplify disruptions to critical inputs and logistics, thereby increasing the likelihood of cascading effects across supply chains. Accounting for such compound and interacting risks is therefore a natural and important extension of this work. Additional extensions include allowing for adaptive supply-chain responses (e.g., substitution and re-routing), incorporating explicit adaptation measures (e.g., protection, hardening, relocation), and using sector-specific damage functions to better capture heterogeneity in vulnerability and improve the precision of the estimates.

References

Aznar-Siguan, G. and D. N. Bresch (2019). Climada v1: a global weather and climate risk assessment platform. *Geoscientific Model Development 12*(7), 3085–3097.

Bressan, G., A. Đuranović, I. Monasterolo, et al. (2024). Asset-level assessment of climate physical risk matters for adaptation finance. *Nature Communications 15*, 5371.

Cardona, O.-D., M. K. van Aalst, J. Birkmann, M. Fordham, G. McGregor, R. Perez, R. S. Pulwarty, E. L. F. Schipper, and B. T. Sinh (2012). Determinants of risk: Exposure and vulnerability. In C. B. Field, V. Barros, T. F. Stocker, D. Qin, D. J. Dokken, K. L. Ebi, M. D. Mastrandrea, K. J. Mach, G.-K. Plattner, S. K. Allen, M. Tignor, and P. M. Midgley (Eds.), *Managing the Risks of Extreme Events and Disasters to Advance Climate Change Adaptation*, pp. 65–108. Cambridge, United Kingdom and New York, NY, USA: Cambridge University Press.

Carvalho, V. M., M. Nirei, Y. U. Saito, and A. Tahbaz-Salehi (2021). Supply chain disruptions: Evidence from the great east japan earthquake. *The Quarterly Journal of Economics 136*(2), 1255–1321.

Colon, C., S. Hallegatte, and J. Rozenberg (2021). Criticality analysis of a country's transport network via an agent-based supply chain model. *Nature Sustainability 4*, 209–215.

Dessertaine, T., J. Moran, M. Benzaquen, and J.-P. Bouchaud (2022). Out-of-equilibrium dynamics and excess volatility in firm networks. *Journal of Economic Dynamics and Control 138*, 104362.

Dix, M., D. Bi, P. Dobrohotoff, R. Fiedler, I. Harman, R. Law, C. Mackallah, S. Marsland, S. O'Farrell, H. Rashid, J. Srbinovsky, A. Sullivan, C. Trenham, P. Vohralik, I. Watterson, G. Williams, M. Woodhouse, R. Bodman, F. B. Dias, C. M. Domingues, N. Hannah, A. Heerdegen, A. Savita, S. Wales, C. Allen, K. Druken, B. Evans, C. Richards, S. M. Ridzwan, D. Roberts, J. Smillie, K. Snow, M. Ward, and R. Yang (2019). Csiro-arccss access-cm2 model output prepared for cmip6 scenariomip.

Eberenz, S., S. Lüthi, and D. N. Bresch (2021). Regional tropical cyclone impact functions for globally consistent risk assessments. *Natural Hazards and Earth System Sciences 21*(1), 393–415.

Emanuel, K. (2011). Global warming effects on U.S. hurricane damage. *Weather, Climate, and Society 3*(4), 261–268.

Fahr, S., R. Senner, and A. Vismara (2024, May). The globalization of climate change: amplification of climate-related physical risks through input-output linkages. ECB Working Paper Series 2942, European Central Bank.

Feehan, C. J., K. Filbee-Dexter, M. S. Thomsen, T. Wernberg, and T. Miles (2024). Ecosystem damage by increasing tropical cyclones. *Communications Earth & Environment 5*, 674.

Gettelman, A., D. N. Bresch, C.-C. Chen, J. E. Truesdale, and J. T. Bacmeister (2018). Projections of future tropical cyclone damage with a high-resolution global climate model. *Climatic Change 146*(3–4), 575–585.

Glanemann, N., S. N. Willner, L. Wenz, R. Bierkandt, and A. Levermann (2016). Abrupt events and the global supply network: A network measure for cascading production losses.

Hallegatte, S. (2008). An adaptive regional input-output model and its application to the assessment of the economic cost of katrina. *Risk Analysis 28*(3), 779–799.

Hallegatte, S. (2014). Modeling the role of inventories and heterogeneity in the assessment of the economic costs of natural disasters. *Risk Analysis 34*(1), 152–167.

Hallegatte, S. and V. Przyluski (2010, December). The economics of natural disasters: Concepts and methods. Policy Research Working Paper 5507, The World Bank.

Hsiang, S. M. and A. S. Jina (2014). The causal effect of environmental catastrophe on long-run economic growth: Evidence from 6,700 cyclones. Working Paper 20352, National Bureau of Economic Research.

Inoue, H. and Y. Todo (2019). Firm-level propagation of shocks through supply-chain networks. *Nature Sustainability 2*, 841–847.

Juhel, S. (2024). Boario: A python package implementing the ario indirect economic cost model. *Journal of Open Source Software 9*(98), 6547.

Kerkhofs, R., M. Bernhofen, M. Borsuk, M. Baer, N. Ranger, W. Schoutens, and G. Shrimali (2025). An asset-level analysis of financial tail risks under extreme weather events. *Environmental Research: Climate 4*(2), 025014.

Klimek, P., S. Poledna, and S. Thurner (2019). Quantifying economic resilience from input–output susceptibility to improve predictions. *Nature Communications 10*.

Knapp, K. R., M. C. Kruk, D. H. Levinson, H. J. Diamond, and C. J. Neumann (2010). The international best track archive for climate stewardship (ibtracs): Unifying tropical cyclone data. *Bulletin of the American Meteorological Society 91*(3), 363 – 376.

Krichene, H., A. Holzhausen, J. Basco Carrera, J. Gröschl, P. Hoffmann, and A. Kuhanathan (2024, October). The global economic ripple effect of cyclones. Technical report, Allianz Research (Allianz SE and Allianz Trade), Munich, Germany.

Krichene, H., T. Vogt, F. Piontek, T. Geiger, C. Schötz, and C. Otto (2023). The social costs of tropical cyclones. *Nature Communications 14*, 7294.

Kuhla, K., S. N. Willner, C. Otto, and A. Levermann (2023, June). Resilience of international trade to typhoon-related supply disruptions. *Journal of Economic Dynamics and Control 151*, 104663.

Kunze, S. (2020). Unraveling the effects of tropical cyclones on economic sectors worldwide: Direct and indirect impacts. *Environmental and Resource Economics*, 545–569.

Le Guenedal, T., P. Drobinski, and P. Tankov (2022). Cyclone generation algorithm including a thermodynamic module for integrated national damage assessment (catherina 1.0) compatible with coupled model intercomparison project (cmip) climate data. *Geoscientific Model Development 15*(21), 8001–8039.

Lehtomaa, J. and C. Renoir (2023, April). The economic impact of tropical cyclones: Case studies in general equilibrium. CER-ETH Economics Working Paper Series 23/382, CER-ETH – Center of Economic Research at ETH Zurich, Zurich, Switzerland. Working Paper 23/382 (April 2023). Full text: https://ethz.ch/content/dam/ethz/special-interest/mtec/cer-eth/cer-eth-dam/documents/working-papers/wp$_2$3$_3$82.*pdf*.

Lenzen, M., A. Geschke, M. D. Abd Rahman, Y. Xiao, J. Fry, R. Reyes, E. Dietzenbacher, S. Inomata, K. Kanemoto, B. Los, D. Moran, H. Schulte in den Bäumen, A. Tukker, T. Walmsley, T. Wiedmann, R. Wood, and N. Yamano (2017). The global mrio lab – charting the world economy. *Economic Systems Research 29*(2), 158–186.

Lenzen, M., A. Malik, S. Kenway, P. Daniels, K. L. Lam, and A. Geschke (2019). Economic damage and spillovers from a tropical cyclone. *Natural Hazards and Earth System Sciences 19*(1), 137–151.

Meiler, S., T. Vogt, N. Bloemendaal, A. Ciullo, C.-Y. Lee, S. J. Camargo, K. Emanuel, and D. N. Bresch (2022). Intercomparison of regional loss estimates from global synthetic tropical cyclone models. *Nature Communications 13*(1), 6156.

Mohan, P. S., B. Ouattara, and E. Strobl (2018). Decomposing the macroeconomic effects of natural disasters: A national income accounting perspective. *Ecological Economics 146*, 1–9.

Otto, C., S. N. Willner, L. Wenz, K. Frieler, and A. Levermann (2017). Modeling loss-propagation in the global supply network: The dynamic agent-based model acclimate. *Journal of Economic Dynamics and Control 83*, 232–269.

Pichler, A., M. Pangallo, R. M. del Rio-Chanona, F. Lafond, and J. D. Farmer (2022). Forecasting the propagation of pandemic shocks with a dynamic input-output model. *Journal of Economic Dynamics and Control 144*, 104527.

Seneviratne, S. I., X. Zhang, M. Adnan, W. Badi, C. Dereczynski, A. Di Luca, S. Ghosh, I. Iskandar, J. Kossin, S. Lewis, F. Otto, I. Pinto, M. Satoh, S. M. Vicente-Serrano, M. Wehner, and B. Zhou (2021). Weather and climate extreme events in a changing climate. In V. Masson-Delmotte, P. Zhai, A. Pirani, S. L. Connors, C. Péan, S. Berger, N. Caud, Y. Chen, L. Goldfarb, M. I. Gomis, M. Huang, K. Leitzell, E. Lonnoy, J. B. Matthews, T. K. Maycock, T. Waterfield, O. Yelekçi, R. Yu, and B. Zhou (Eds.), *Climate Change 2021: The Physical Science Basis. Contribution of Working Group I to the Sixth Assessment Report of the Intergovernmental Panel on Climate Change*, pp. 1513–1766. Cambridge, United Kingdom and New York, NY, USA: Cambridge University Press.

Shughrue, C., B. Werner, and K. C. Seto (2020). Global spread of local cyclone damages through urban trade networks. *Nature Sustainability 3*, 606–613.

Simpson, N. P., K. J. Mach, A. Constable, J. Hess, R. Hogarth, M. Howden, J. Lawrence, R. J. Lempert, V. Muccione, B. Mackey, M. G. New, B. O'Neill, F. Otto, H.-O. Pörtner, A. Reisinger, D. Roberts, D. N. Schmidt, S. Seneviratne, S. Strongin, M. van Aalst, E. Totin, and C. H. Trisos (2021). A framework for complex climate change risk assessment. *One Earth 4*(4), 489–501. Perspective.

Tukker, A. and E. Dietzenbacher (2013). Global multiregional input-output framework: An introduction and outlook. *Economic Systems Research 25*(1), 1–19.

Wang, B.-W., Y. He, W.-H. Wu, and F. Teng (2025). Quantifying indirect economic losses from extreme events to inform global and local adaptation strategies. *Advances in Climate Change Research 16*(4), 674–687.

6 Appendix : Data sources and description

6.1 MRIO data

We use the Gloria Multi-Regional Input-Output (MRIO) (Lenzen et al. (2017)) database to characterize inter-industry linkages at the sector–region level. For a general presentation of MRIO accounting and notation, see Tukker and Dietzenbacher (2013). In out setting, we adopt the following notation: the economy is composed of a set of industries $\mathcal{I} = \{I_1, \ldots, I_M\}$ of size M, where each industry corresponds to a specific sector in a given region. Unless stated otherwise, we use $i \in \{1, \ldots, M\}$ both to denote industry I_i and its index. An MRIO table can be represented by the following objects:

- Intermediate transactions: $\mathbf{Z} \in \mathbb{R}^{M \times M}$ is the matrix of intermediary input flows, where $z_{i,j}$ denotes the monetary value of inputs produced by industry i and used as intermediate consumptions by industry j.
- Final demand: $\mathbf{y} \in \mathbb{R}^M$ is the vector of final demand, with elements y_j
- Gross output: $\mathbf{x} \in \mathbb{R}^M$ is the vector of gross output (total production), with elements x_j
- Technical coefficients: $\mathbf{A} \in \mathbb{R}^{M \times M}$ is the matrix of technical coefficients, defined by $a_{i,j} = \frac{z_{i,j}}{x_j}$. Each element $a_{i,j}$ measures the amount of output from industry i required to produce one unit of output of industry j.
- $\mathbf{va} \in \mathbb{R}^M$ the vector of value added, with elements va_i.
- $\mathbf{K} \in \mathbb{R}^M$ the vector of total capacity from the MRIO tables, with elements K_i

The vector of total capacity is not directly provided by the MRIO tables. We follow Hallegatte (2008), and initialize it at $\mathbf{K} = 4\mathrm{VA}$

At equilibrium, we following accounting equilibrium holds:

$$x_i = \sum_{j=1}^{M} z_{i,j} + y_i = \sum_{k=1}^{M} z_{k,i} + \mathrm{va}_i,\ \forall i \in [1, \ldots, M]$$

6.2 CATHERINA model

The Cyclone generation Algorithm including a THERmodynamic module for Integrated National damage Assessment (CATHERINA) model generates synthetic cyclone tracks, sensitive to local climate conditions. The algorithm is composed of three main steps: (i) genesis of cyclones, (ii) displacement of the cyclone and (iii) intensification of the wind-speed, summarized in Figure 8. The first two stages are statistical and calibrated on the historical observations. This means that the the climate variables defining the scenario do not affect either the number of cyclones generated or their trajectories. The intensification step is based on a physical model, and depends on four climate variables: mean sea-level pressure, tropospheric temperature, sea-surface temperature, and relative humidity.

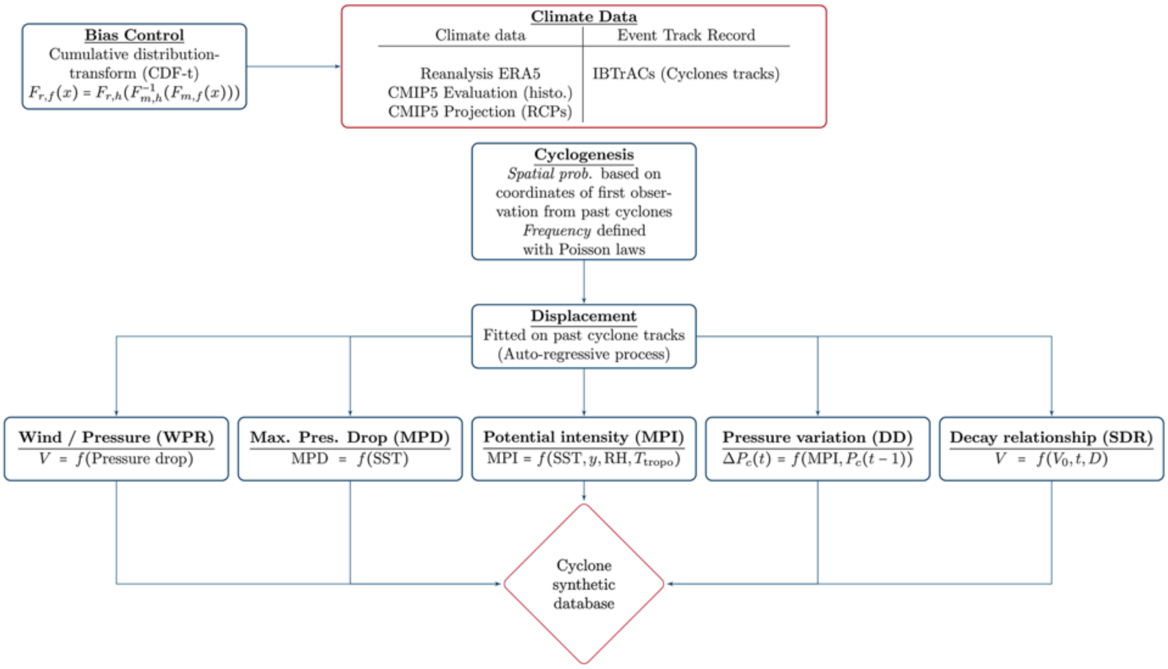

Figure 8: Schematic representation of the cyclone generation algorithm. Source: Adapted from Le Guenedal et al. (2022)

In Figure 9, we compare the simulated TCs to observed events from IBTrACS. For each basin, we construct the empirical distribution of cyclone intensity by computing the frequency of events across Saffir–Simpson categories for both the observations and the simulations. For the simulated series, the error bars reflect cross-simulation variability across the 100 simulations. Overall, the simulated category frequencies are broadly consistent with the IBTrACS benchmark. The main discrepancies arise in the North and South Indian basins. These basins feature comparatively few events in both the observed record and in our simulations, so category shares are estimated from small samples and are therefore more volatile. Consequently, deviations in these basins should be interpreted with caution.

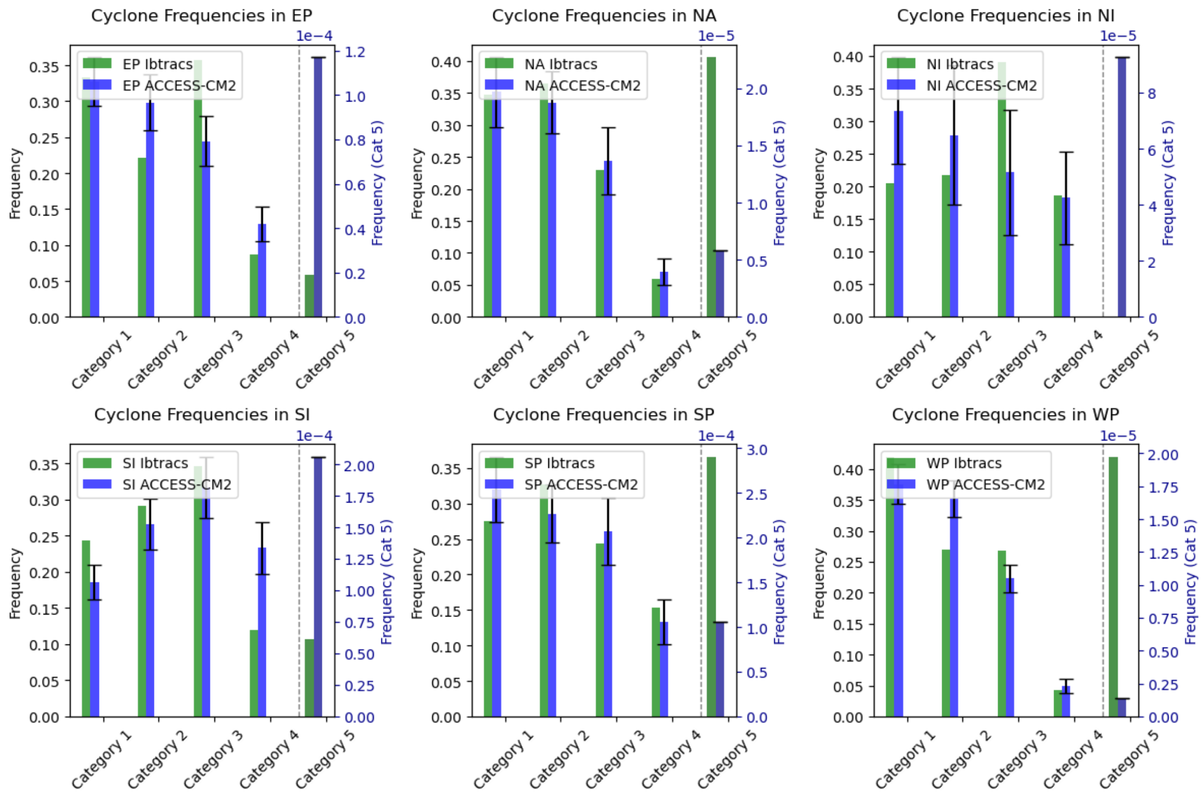

Figure 9: Validation of simulated TC categories against IBTrACS

7 Appendix : Database construction and industry damage estimation

7.1 Spatial distribution of production

We use asset-level geolocation data from Climate TRACE to approximate the spatial distribution of region–sector production. The production of prod_ℓ the assets ℓ is provided in physical unit, whereas the total production and capacity from the input-output tables are provided in monetary terms. We use the following steps to allocate a monetary production to each asset:

- Step 1: compute the size (respective to the production of its industry) of each asset
- Step 2: split the monetary industry production and capacity based on the size

This approach relies on two key assumptions: (i) the Climate TRACE asset database is sufficiently complete so that physical production shares provides a meaningful proxy for the within-industry spatial distribution, and (ii) physical production is an appropriate proxy for "size" when apportioning monetary output and capacity (alternatives include installed capacity or capital stock when available).

Compute the size of each asset For each industry i, let the set of assets mapped to that industry be:

$$\mathcal{A}_i := \{ a_\ell \in \mathcal{A} \ : \ I(a_\ell) = i \}$$

We define the weight of asset a_l as its share of total baseline production within its industry:

$$\alpha_l = \frac{\text{prod}_\ell}{\sum_{k \in \mathcal{A}_{I(a_\ell)}} \text{prod}_k}$$

Compute the production split For each asset, we compute the monetary production and capacity:

$$x_\ell^{\text{asset}} = \alpha_\ell \, x_i, \qquad K_\ell^{\text{asset}} = \alpha_\ell \, K_i.$$

7.2 Industry-level damage fraction estimation

The damages are computed at asset-level and then aggregated at industry level. The industry level damages thus account for the spatial distribution of capacities. The steps to compute sector-level tropical cyclone linked impacts are the following:

1. Estimate the number of events per asset and define the effective wind
2. Compute the asset-level damages
3. Aggregate asset-level damages at sector level

TO compute the asset-level fraction of damage, we use the wind-damage function of Emanuel (2011), with parameter calibration from Eberenz et al. (2021):

$$f(v, v_h^r) = \frac{\max(v - v_0, 0)^3}{(v_h^r - v_0)^3 + \max(v - v_0, 0)^3},$$

with $v_0 = 92.5\,\text{km}\,\text{h}^{-1}$ and v_h^r a region-specific calibrated parameter.

Step 1: Estimate the wind used to compute damages An event is defined as the crossing of a wind track over an asset position P_l^{asset}. To account for the size of the tropical cyclone, we define a buffer zone around the asset position as the set of locations located within $r = 200$ km of P_l^{asset}. With $d(.,.)$ by a distance function, we define buffer zone is defined as:

$$B_r(P_l^{\text{asset}}) = \{p \in \mathbb{R}^2 : d(p, P_l^{\text{asset}}) \leq r\}$$

The set of track time-steps where the cyclone is within the buffer is :

$$\mathcal{S}_{k,l} = \{t \in [0, T], : P_{t,k}^{\text{cyclone}} \in B_r(P_l^{\text{asset}})\}$$

Conditional on an event taking place ($\mathcal{S}_{k,l} \neq \emptyset$), we define the wind value used to compute the damage on asset l from cyclone k as follows:

- For empirical observations (IBTraCKS) : the maximum value of wind

$$\tilde{v}_{k,\ell} = \max(v_{t,k} : t \in \mathcal{S}_{k,\ell})$$

- For simulated values (CATHERINA), given the uncertainty on both the track positions and wind values, we select a quantile of all values in buffer:

$$\tilde{v}_{k,\ell} = \text{Quantile}_q(v_{t,k} : t \in \mathcal{S}_{k,\ell})$$

  This quantile q is selected to minimize the distance between the empirical distribution and the distribution of simulated losses on the historical data.

Step 2: Compute the asset-level damages The fraction of damages to asset l from cyclone k is:

$$\epsilon_{k,\ell} = f(\tilde{v}_{k,\ell}, v_h^{R(\ell)})$$

Step 3: Aggregate asset-level damages at sector level To obtain damages at the industry level, we compute the maximum asset loss over the set of cyclones occurring in year t. Let $\mathcal{TC}_t$ denote the set of cyclones in year t. The annual industry-level fraction of damage to capital linked to tropical cyclones is thus:

$$\zeta_i(t) = \frac{\sum_{\ell \in \mathcal{A}_i} \left(\max_{k \in \mathcal{TC}_t} \epsilon_{k\ell}\right) K_\ell}{\sum_{\ell \in \mathcal{A}_i} K_\ell}.$$

The industry-level damage fraction $\zeta_i(t)$ is then used as an input to the production network model to parametrize tropical-cyclone-induced shocks. Using notations from the MRIO data, we model the shock as a proportional reduction in productive capital, so that the maximum feasible output at t_0 satisfies

$$x_i(t_\tau) \ \leq \ \big(1 - \zeta_i(t_\tau)\big)\, \nu_i\, K_i(t_\tau) = \big(1 - \zeta_i(t_\tau)\big)\, x^K(t_\tau)$$

where ν_i is the capital-to-output conversion rate. We assume ν_i is time-invariant and initialize it from the baseline steady state as $\nu_i = \frac{x_i(0)}{K_i(0)}$. $x_i^K(t)$ thus represents the maximum of production that is achievable with capacity $K_i(t)$.

7.3 Industry-level damage benchmarking

In Figure 10, we compare observed and simulated annual damages by industry, colouring observations by region. Overall, the model reproduces the empirical pattern reasonably well, with a limited number of outliers—most notably at low levels of observed damages. In these cases, discrepancies largely reflect sparse exposure in the ClimateTRACE asset database: when only a few assets represent an industry–region cell, simulated impacts can be disproportionately large relative to the observed benchmark. We also observe a tendency to overestimate damages for Japan (grey points). This appears to be driven by upward-biased wind speeds in Japan in the CATHERINA hazard module. Using alternative climate models should mitigate this issue; and this inclusion is ongoing.

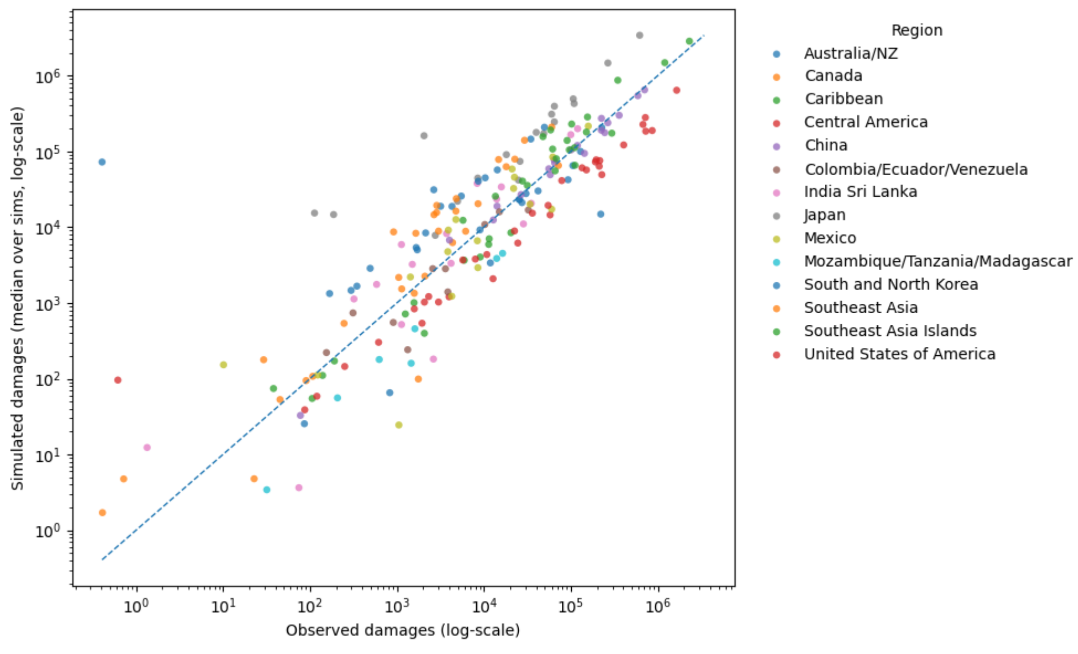

Figure 10: Comparison of Observed vs Simulated Damage Amounts by industry. Note: Observed damages are the median annual damage amount across years. Simulated damages are the mean across simulations of each simulation's median annual damage amount.

Figure 11 reports the distribution of industry-level damage ratios, where for each period we summarize damages by taking the median across years. As expected, damage ratios are larger and more dispersed than in the global aggregate, reflecting substantial heterogeneity in exposure across industries. The distribution shifts upward over time, with the upper tail indicating roughly a doubling of losses in the most extreme cases. Importantly, at the industry level the simulated historical period is broadly consistent with the observed benchmark, suggesting that the model captures the central tendency of sectoral damages.

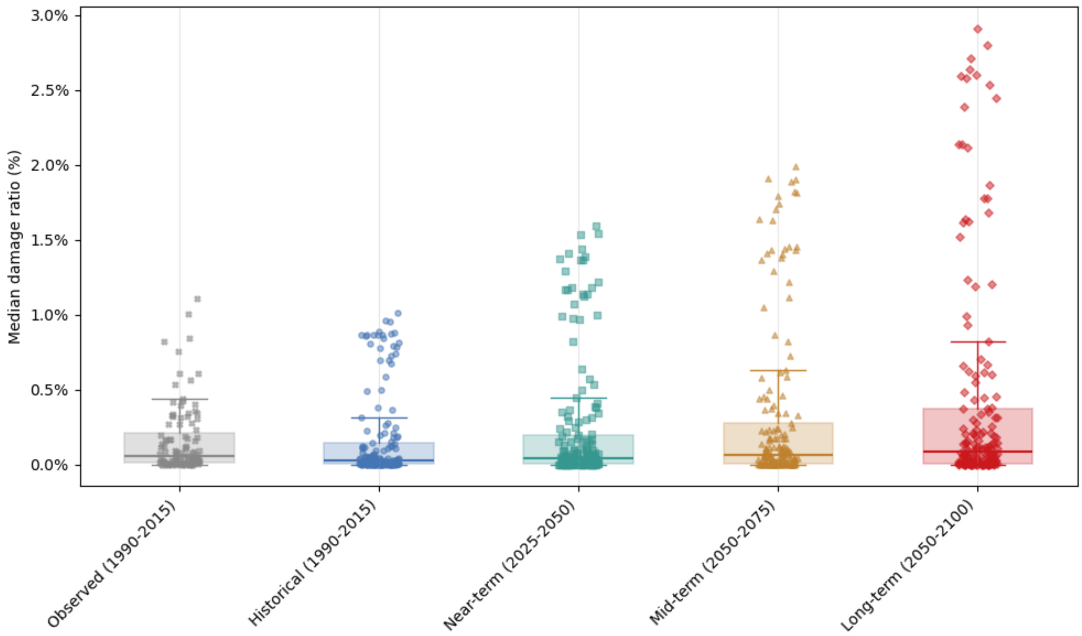

Figure 11: Distribution of median annual damages by industries. Note: for simulated periods, we average across simulation.

8 Appendix : Dynamic MRIO model

8.1 Notation summary

Symbol	Description
$\mathcal{R}$	Set of regions, $r = 1, \ldots, R$
$\mathcal{S}$	Set of sectors (goods), $s = 1, \ldots, S$
$\mathcal{I} = \mathcal{R} \times \mathcal{S}$	Set of industries, $i = (r, s)$
$r(i)$, $s(i)$	Region and sector of industry i
$\mathcal{I}_r^{\mathrm{T}}$	Tradable industries in region r
$\mathcal{I}_r^{\mathrm{N}}$	Non–tradable industries in region r
k	Generic sector / input good index
i	Generic origin industry index
j	Generic destination industry index
t	Time period, $t = 0, 1, 2, \ldots$
$x_i(t)$	Output of industry i in period t
$K_i(t)$	Captial of industry i in period t
ν_i	output-to-capacity ratio of industry i
$p_i(t)$	Producer price of good i
$p_{0,r}(t)$	Wage in region r
$a_{k,j}$	Input coefficient of sector k in industry j (per unit output)
$a_{\ell,j}$	Labour coefficient of industry j (per unit output)
$\epsilon_j(t)$	Productivity of industry j
$\Omega_{k,j}(t)$	Inventory of sector-k good held by industry j at t
$\hat{\Omega}_{k,j}$	Target inventory for sector-k good of industry j
σ_k	Inventory decay rate for good k
τ	Speed of inventory adjustment parameter
$L_r^s(t)$	Household labour supply in region r
$L_r^d(t)$	Total labour demand in region r
$\ell_i^d(t)$	Desired labour demand of industry i
$\ell_i(t)$	Actual labour hired by industry i
$L_{0,r}$	Labour supply scale in region r
$\theta_{r,i}$	Preference weight of good i in region r
Γ_r, ϕ_r	Labour disutility parameters in region r
$S_r(t)$	Financial savings of region-r household at t
$B_r(t)$	Budget of region-r household at t
r_r	Interest rate on regional savings
$z_{k,j}^d(t)$	Desired input from sector k into industry j
$z_{i,j}^d(t)$	Desired intermediate flow from industry i to j
$z_{i\to j}(t)$	Actual intermediate delivery from i to j
$z_{k\to j}(t)$	Actual sector-k deliveries into j, $\sum_{i:s(i)=k} z_{i\to j}$
$z_{k,j}^a(t)$	Available sector-k input for j: $z_{k,j}^a = \Omega_{k,j} + \sum_{i:s(i)=k} z_{i\to j}$
$u_{k,j}(t)$	Used sector-k input for j: $u_{k,j} = \min(z_{k,j}^a, z_{k,j}^d)$
$y_{i,r}^{c,d}(t)$	Desired household consumption of good i in region r
$y_{i,r}^{g,d}(t)$	Desired exogenous (e.g. government) demand for i in region r
$y_{i,r}^d(t)$	Total desired final demand for i in region r $(c + g)$
$y_{i,r}(t)$	Actual total final demand for i in region r
$y_i^d(t)$	Total desired final demand for good i, $\sum_r y_{i,r}^d$
$y_i(t)$	Total actual final demand for good i, $\sum_r y_{i,r}$

Symbol	Description
$\kappa_r(t)$	Transport availability in region r (fraction of normal capacity)
$\chi_i(t)$	Transport factor for industry i: $= \kappa_{r(i)}$ if $i \in \mathcal{I}^{\mathrm{T}}_{r(i)}$, else 1
$\widetilde{z}^d_{i,j}(t)$	Transport–filtered desired intermediate flow from i to j
$\widetilde{y}^{q,d}_{i,r}(t)$	Transport–filtered desired final demand (type $q \in \{c, g\}$) for i in r
$\widetilde{y}^d_i(t)$	Total transport–filtered final demand for i: $\sum_r \sum_q \widetilde{y}^{q,d}_{i,r}$
$\widetilde{D}_i(t)$	Total transport–filtered demand for good i
$S_i(t)$	Supply of good i available for sale (e.g. $S_i = x_i$)
$\lambda_i(t)$	Goods rationing factor for supplier i: $\lambda_i = \min\{1, S_i/\widetilde{D}_i\}$
$\phi_r(t)$	Household budget rationing factor in region r
$\widetilde{C}_r(t)$	Notional cost of desired consumption after physical rationing
$\Pi_i(t)$	Realised profit of industry i
$\mathcal{E}_i(t)$	Realised imbalance between supply and actual demand for i
$\mathcal{G}_i(t)$	Total realised revenues of industry i
$\mathcal{L}_i(t)$	Total realised costs of industry i
$\mathcal{S}_i(t)$	Supply aggregate for i (e.g. $\mathcal{S}_i = S_i$)
$\mathcal{D}_i(t)$	Demand aggregate for i (e.g. $\mathcal{D}_i = \widetilde{D}_i$)
$\mathbb{E}_t[\cdot]$	Naive one–period–ahead expectation at t
β, β'	Output adjustment parameters (production target rule)
α, α'	Price adjustment parameters (price update rule)
ω	Wage adjustment parameter (Phillips curve)

8.2 Agents, goods and indexing

Time is discrete, $t = 0, 1, 2, \dots$. To distinguish between desired (planned) quantities and actual deliveries, desired quantities carry a superscript d, while actual deliveries between industries are indexed by $i \to j$.

Regions and sectors. We consider a finite set of regions $\mathcal{R}$, indexed by $r = 1, \dots, R$, and a finite set of sectors $\mathcal{S}$, indexed by $s = 1, \dots, S$. An industry is a region–sector pair $i = (r, s) \in \mathcal{I} := \mathcal{R} \times \mathcal{S}$. We denote by $r(i)$ and $s(i)$ the region and sector of industry i.

Goods and factors. Each sector $k \in \mathcal{S}$ corresponds to a differentiated good. In each region r, there is a representative household supplying labour and consuming sectoral goods. Labour is region–specific and not mobile across regions. We denote by $x_i(t)$ the output of industry i at time t, and by $p_i(t)$ the corresponding producer price. Wages in region r are denoted by $p_{0,r}(t)$.

Technology, production and inventories. Production technology is sector–specific. Let $a_{k,j} \geq 0$ be the technical coefficient measuring the quantity of input from sector k needed per unit of (effective) output in industry j, and $a_{\ell,j} \geq 0$ the labour coefficient of industry j. Each industry j has productivity $\epsilon_j(t) > 0$ and, in the notional Leontief technology, inputs and labour consistent with a realised output $x_j(t)$ would satisfy

$$z_{k,j}(t) = a_{k,j}\,\frac{x_j(t)}{\epsilon_j(t)}, \qquad \ell_j(t) = a_{\ell,j}\,\frac{x_j(t)}{\epsilon_j(t)},$$

where $z_{k,j}(t)$ is the (sector–level) quantity of good k used by industry j. All industries hold inventories of goods by sector: for each input sector k,

$$\Omega_{k,j}(t)$$

denotes the stock of good of sector k available to industry j at the beginning of period t (inventories do not distinguish the geographic origin of the good). Each industry has a target stock

$\hat{\Omega}_{k,j}$. We follow Hallegatte (2008) and initialise it to the inventory needed to produce for 3 units of time.

Households, final demand and savings. In each region r, a representative household chooses consumption $y_{i,r}^{c,d}(t)$ of each industry–good i and labour supply $L_r^s(t)$, and holds financial savings $S_r(t)$. Household consumption is endogenous and is determined by solving the consumption maximisation under budget constraint problem of the consumer. We denote by $y_{i,r}^{g,d}(t)$ any exogenous final demand (e.g. government) for good i in region r. Final demand for goods of industry i by region r is thus given by:

$$y_{i,r}^{d}(t) = y_{i,r}^{c,d}(t) + y_{i,r}^{g,d}(t).$$

Total desired final demand for good i is

$$y_i^d(t) = \sum_{r\in\mathcal{R}} y_{i,r}^d(t).$$

Households' optimisation problem. In each region r, the representative household maximises per–period utility

$$\mathcal{U}_r(t) = \sum_{i\in\mathcal{I}} \theta_{r,i} \log y_{i,r}^c(t) - \frac{\Gamma_r}{1+\phi_r}\left(\frac{L_r^s(t)}{L_{0,r}}\right)^{1+\phi_r}, \tag{7}$$

subject to the budget constraint

$$\sum_{i\in\mathcal{I}} p_i(t) y_{i,r}^c(t) = p_{0,r}(t) L_r^s(t) + S_r(t), \tag{8}$$

where $\theta_{r,i}$ are preference weights ($\sum_i \theta_{r,i} = 1$), $L_{0,r}$ is a scale of labour supply and $\Gamma_r, \phi_r > 0$ parameterise labour disutility. The household chooses desired consumption $y_{i,r}^{c,d}(t)$ and labour supply $L_r^s(t)$, anticipating that all goods markets clear and labour demand in their region fully absorbs their supply (optimistic expectations).

Supply and demand dynamics. Figure 13 presents a schematic overview of the supply and demand mechanisms.

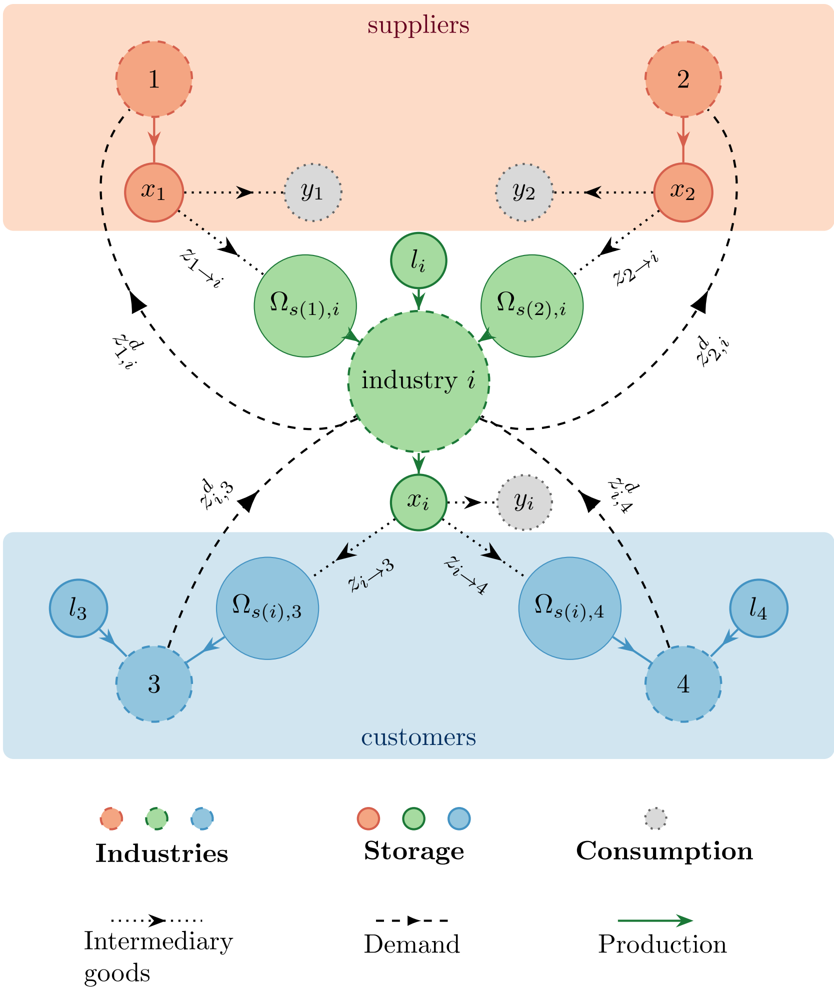

Figure 12: Schematic representation of the supply, demand and inventory roles

8.3 Timeline of events

Each period t is divided into three stages: (i) firms' planning; (ii) exchanges and price/wage updates; (iii) production, inventory updates and capital/emissions dynamics.

8.3.1 Firms' planning

At the beginning of stage 1 of period t, past output $x_i(t)$, prices $p_i(t)$ and wages $p_{0,r}(t)$ are known, while current–period demands and trades are not. Firms form naive one–period–ahead expectations using lagged realised or desired quantities, depending on the variable. We denote expectations conditional on $(x(t), p(t), p_0(t))$ by $\mathbb{E}_t[\cdot]$.

Expected profit and imbalances. For each industry i, define expected profits and expected imbalances as

$$\begin{aligned}\mathbb{E}_t[\Pi_i(t)] = p_i(t)\Big(\sum_{j\in\mathcal{I}}\mathbb{E}_t[z_{i\to j}(t)] + \mathbb{E}_t[y_i(t)]\Big)\\ - \Big(\sum_{j\in\mathcal{I}} p_j(t)\mathbb{E}_t[z_{j\to i}(t)] + p_{0,r(i)}(t)\mathbb{E}_t[\ell_i(t)]\Big),\\ \mathbb{E}_t[\mathcal{E}_i(t)] = x_i(t) - \Big(\sum_{j\in\mathcal{I}}\mathbb{E}_t[z_{i\to j}(t)] + \mathbb{E}_t[y_i(t)]\Big).\end{aligned}$$

We also define expected total revenues and costs

$$\mathbb{E}_t[\mathcal{G}_i(t)] = p_i(t)\Big(\sum_{j\in\mathcal{I}} \mathbb{E}_t[z_{i\to j}(t)] + \mathbb{E}_t[y_i(t)]\Big), \quad \mathbb{E}_t[\mathcal{L}_i(t)] = \sum_{j\in\mathcal{I}} p_j(t)\mathbb{E}_t[z_{j\to i}(t)] + p_{0,r(i)}(t)\mathbb{E}_t[\ell_i(t)],$$

and expected supply/demand aggregates $\mathbb{E}_t[\mathcal{S}_i(t)]$, $\mathbb{E}_t[\mathcal{D}_i(t)]$ for normalisation, with $\mathcal{S}_i(t)$ and $\mathcal{D}_i(t)$ defined below.

Expectations are *naive*. For trade and final demand flows with a desired counterpart, we set

$$\mathbb{E}_t[z_{i\to j}(t)] = z^d_{i,j}(t-1), \qquad \mathbb{E}_t[y_i(t)] = y^d_i(t-1),$$

and similarly for labour demand,

$$\mathbb{E}_t[\ell_i(t)] = \ell^d_i(t-1).$$

Other expectation forms could be implemented (adaptive, forecast, etc.).

Production targets. Firms update their target output $\hat{x}_i(t+1)$ according to a behavioural rule combining expected profitability and expected excess supply:

$$\log\left(\frac{\hat{x}_i(t+1)}{x_i(t)}\right) = \beta\,\frac{\mathbb{E}_t[\Pi_i(t)]}{\mathbb{E}_t[\mathcal{G}_i(t)] + \mathbb{E}_t[\mathcal{L}_i(t)]} - \beta'\,\frac{\mathbb{E}_t[\mathcal{E}_i(t)]}{\mathbb{E}_t[\mathcal{S}_i(t)] + \mathbb{E}_t[\mathcal{D}_i(t)]}, \tag{9}$$

with adjustment parameters $\beta, \beta' \geq 0$.

Desired inputs and inventories by sector. Given the target $\hat{x}_j(t+1)$, desired input quantities by sector k and desired labour demand are

$$z^d_{k,j}(t) = a_{k,j}\,\frac{\hat{x}_j(t+1)}{\epsilon_j(t)} + \frac{1}{\tau}\big(\hat{\Omega}_{k,j} - \Omega_{k,j}(t)\big), \tag{10}$$

$$\ell^d_j(t) = a_{\ell,j}\,\frac{\hat{x}_j(t+1)}{\epsilon_j(t)}, \tag{11}$$

where $\tau > 0$ governs the speed of inventory adjustment towards the notional target stock $\hat{\Omega}_{k,j}$.

Intermediate demand by sector is then split back to intermediate demand by industry, following fixed initial shares. For each sector k and industry i with $s(i) = k$, we define a time–invariant share

$$\phi_{i|k,j} = \frac{z_{i,j}(0)}{\sum_{i':s(i')=k} z_{i',j}(0)}$$

for some reference destination j, and set

$$z^d_{i,j}(t) = \phi_{i|k,j}\, z^d_{k,j}(t), \qquad \text{for all } j \text{ and } k = s(i).$$

8.3.2 Exchanges, rationing, profits and price/wage updates

Labour market. Given labour demands $\{\ell^d_i(t)\}_{i\in\mathcal{I}}$ and household labour supply $L^s_r(t)$, the total labour demand in region r is

$$L^d_r(t) = \sum_{i\in\mathcal{I}:r(i)=r} \ell^d_i(t).$$

Actual labour hired by industry i is rationed if demand exceeds supply:

$$\ell_i(t) = \ell^d_i(t)\,\lambda_{r(i)}(t), \quad \lambda_r(t) := \min\left(1, \frac{L^s_r(t)}{L^d_r(t)}\right). \tag{12}$$

The wage $p_{0,r}(t)$ is updated via a Phillips–curve rule,

$$\log\left(\frac{p_{0,r}(t+1)}{p_{0,r}(t)}\right) = \omega\,\frac{L_r^d(t) - L_r^s(t)}{L_r^d(t) + L_r^s(t)}, \tag{13}$$

with $\omega \geq 0$.

The realised labour income in region r is $p_{0,r}(t)\sum_{i:r(i)=r}\ell_i(t)$ and the current budget is

$$B_r(t) = S_r(t) + p_{0,r}(t)\sum_{i:r(i)=r}\ell_i(t). \tag{14}$$

Region–level transport availability and tradable industries. We assume that transport disruptions (e.g. partial port closures) are captured by a region–level availability parameter. For each region $r \in \mathcal{R}$ and time t, let

$$\kappa_r(t) \in [0,1]$$

denote the fraction of normal transport capacity that is available for both imports and exports. For example, $\kappa_r(t) = 0.6$ means that ports in region r operate at 60% of their baseline capacity.

Not all industries are affected by these constraints. We distinguish a subset of tradable industries,

$$\mathcal{I}^{\mathrm{T}}$$

for which transport constraints apply (e.g. manufacturing, agriculture, mining), and non–tradable industries

$$\mathcal{I}^{\mathrm{N}} := \mathcal{I} \setminus \mathcal{I}_r^{\mathrm{T}}$$

(e.g. local services) for which they do not.

We define a region–level transport factor for each industry i as

$$\chi_i(t) := \begin{cases} \kappa_{r(i)}(t) & \text{if } i \in \mathcal{I}^{\mathrm{T}}, \\ 1 & \text{if } i \in \mathcal{I}^{\mathrm{N}}. \end{cases}$$

Symmetric import and export filtering. Let $z_{i,j}^d(t)$ denote the planned intermediate flow from industry i to industry j at time t, and $y_{i,r}^{q,d}(t)$ the planned final demand of type $q \in \{c,g\}$ for good i in region r.

Imports into j from foreign suppliers are filtered by the availability of transport in the origin and destination regions:

$$\widetilde{z}_{i,j}^d(t) := \begin{cases} \chi_j(t)\chi_i(t)\,z_{i,j}^d(t) & \text{if } r(i) \neq r(j), \\ z_{i,j}^d(t) & \text{if } r(i) = r(j), \end{cases}$$

i.e. planned foreign intermediate inputs into j are scaled down to a fraction $\chi_j(t)\chi_i(t)$ when either the origin or the destination belongs to a tradable sector in a region with limited port availability, while domestic intermediate flows are unaffected.

Final demand is affected similarly:

$$\widetilde{y}_{i,r}^{q,d}(t) := \begin{cases} \kappa_r(t)\chi_i(t)\,y_{i,r}^{q,d}(t) & \text{if } i \in \mathcal{I}^{\mathrm{T}} \text{ and } r(i) \neq r, \\ y_{i,r}^{q,d}(t) & \text{if } r(i) = r, \end{cases}$$

for $q \in \{c,g\}$.

Thus, for industries $i \in \mathcal{I}^{\mathrm{T}}$ in a region r with $\kappa_r(t) < 1$, both foreign intermediate flows ($z_{i,j}^d$ with $r(j) \neq r(i)$) and foreign final demand ($y_{i,r'}^{q,d}$ with $r' \neq r(i)$) are proportionally reduced by a factor taking into account physical limits on imports and exports. Non–tradable industries $i \in \mathcal{I}^{\mathrm{N}}$ are not directly affected by port capacity reductions and keep $\chi_i(t) = 1$.

Rationing of goods under transport and supply constraints In the subsequent step, the effective domestic and foreign demands seen by each supplier i are constructed from the filtered flows $\widetilde{z}^{d}_{i,j}(t)$ and $\widetilde{y}^{q,d}_{i,r}(t)$, and are then matched against available supply $x_i(t)$, with any residual production flowing into inventories of buyers.

Step 1: effective domestic and foreign demand seen by each supplier. From the point of view of a supplier i, the effective demand that can in principle be received, given import constraints in destination regions and export constraints in its own region, is constructed by aggregating the filtered bilateral flows $\widetilde{z}^{d}_{i,j}(t)$ and the filtered final demands $\widetilde{y}^{q,d}_{i,r}(t)$. We define total transport–filtered final demand for good i as

$$\widetilde{y}^{d}_{i}(t) = \sum_{r\in\mathcal{R}} \sum_{q\in\{c,g\}} \widetilde{y}^{q,d}_{i,r}(t),$$

and total transport–filtered demand as

$$\widetilde{D}_i(t) = \widetilde{y}^{d}_{i}(t) + \sum_{j\in\mathcal{I}} \widetilde{z}^{d}_{i,j}(t).$$

The total supply of good i available for sale in period t is given by current output:

$$S_i(t) := x_i(t).$$

Step 2: rationing against available supply. When $S_i(t) < \widetilde{D}_i(t)$, actual deliveries are rationed proportionally across all domestic and foreign uses. We define the rationing factor:

$$\lambda_i(t) := \min\left(1,\ \frac{S_i(t)}{\widetilde{D}_i(t)}\right).$$

Actual intermediate deliveries after physical (supply) rationing are

$$z_{i\to j}(t) = \lambda_i(t)\, \widetilde{z}^{d}_{i,j}(t),$$

and the notional consumption and government flows after physical rationing are

$$y^{q,\mathrm{phys}}_{i,r}(t) = \lambda_i(t)\, \widetilde{y}^{q,d}_{i,r}(t), \qquad q \in \{c, g\}.$$

Step 3: rationing against household budget constraints. Even if physical supply is sufficient, household demand can be constrained by the budget $B_r(t)$. Let $y^{c,\mathrm{phys}}_{i,r}(t)$ be the consumption quantity of good i in region r after physical rationing (as above), and let

$$C^{\mathrm{phys}}_{r}(t) = \sum_{i\in\mathcal{I}} p_i(t)\, y^{c,\mathrm{phys}}_{i,r}(t)$$

be its notional cost. Actual consumption is limited by the household budget rationing factor:

$$\phi_r(t) := \min\left(1,\ \frac{B_r(t)}{C^{\mathrm{phys}}_{r}(t)}\right),$$

and actual final consumption flows are

$$y^{c}_{i,r}(t) = \phi_r(t)\, y^{c,\mathrm{phys}}_{i,r}(t).$$

Government (or other exogenous) final demand is assumed not to be subject to a budget constraint and is given by

$$y^{g}_{i,r}(t) = y^{g,\mathrm{phys}}_{i,r}(t).$$

Step 4: aggregation of actual final demand. Total actual final demand received by industry i is

$$y_i(t) = \sum_{r\in\mathcal{R}} \big(y^c_{i,r}(t) + y^g_{i,r}(t)\big).$$

In the limit $\kappa_r(t) = 1$ for all r, this rationing scheme reduces to standard proportional rationing of demand when current output $x_i(t)$ is insufficient to meet total planned demand.

Profits, imbalances and price updates. Given realised trades, the profit of industry i is

$$\Pi_i(t) = p_i(t)\Big(\sum_{j\in\mathcal{I}} z_{i\to j}(t) + y_i(t)\Big) - \Big(\sum_{j\in\mathcal{I}} p_j(t) z_{j\to i}(t) + p_{0,r(i)}(t)\ell_i(t)\Big). \tag{15}$$

The realised imbalance between supply and realised demand is

$$\mathcal{E}_i(t) = S_i(t) - \left[\sum_{j\in\mathcal{I}} z_{i\to j}(t) + y_i(t)\right]. \tag{16}$$

Total realised revenues and costs are

$$\mathcal{G}_i(t) = p_i(t)\Big(\sum_{j\in\mathcal{I}} z_{i\to j}(t) + y_i(t)\Big), \quad \mathcal{L}_i(t) = \sum_{j\in\mathcal{I}} p_j(t) z_{j\to i}(t) + p_{0,r(i)}(t)\ell_i(t),$$

and we define realised supply and demand aggregates as

$$\mathcal{S}_i(t) := S_i(t), \quad \mathcal{D}_i(t) := \sum_{j\in\mathcal{I}} z_{i\to j}(t) + y_i(t).$$

Prices respond to profits and imbalances according to

$$\log\left(\frac{p_i(t+1)}{p_i(t)}\right) = -\,\alpha\,\frac{\Pi_i(t)}{\mathcal{G}_i(t)+\mathcal{L}_i(t)} - \,\alpha'\,\frac{\mathcal{E}_i(t)}{\mathcal{S}_i(t)+\mathcal{D}_i(t)}, \tag{17}$$

with $\alpha, \alpha' \geq 0$.

8.3.3 TC related damages and reconstruction

We assume that an unforeseen shock arrives at time t. The capital of industry i becomes:

$$K_i(t) = (1-\zeta_i(t))K(t-1)$$

The maximum production of industry i will thus be limited by $\nu_i K_i(t)$.

Reconstruction starts in $t+1$ and generated a supplementary reconstruction demand for specific sectors.

8.3.4 Production and inventories by sector

After trades are realised and wages/prices updated, firms observe the effective quantities of labour and intermediates available for production.

Available and used inputs by sector. For each industry $j = (r, s)$, the realised intermediate deliveries from industry i to j are $z_{i \to j}(t)$. We define the (sector–level) realised deliveries of good k to j as

$$z_{k,j}(t) := \sum_{i \in \mathcal{I}: s(i)=k} z_{i \to j}(t).$$

The effective quantity of input from sector k available to j is then

$$z^a_{k,j}(t) = z_{k,j}(t) + \Omega_{k,j}(t). \tag{18}$$

Labour is non–storable, so the available labour input for production is $\ell_j(t)$.

Used inputs are defined as

$$u_{k,j}(t) = \min\big(z^a_{k,j}(t),\, z^d_{k,j}(t)\big), \tag{19}$$

i.e. industry j cannot use more of sector k than what is available, nor more than its desired use.

Leontief production. We assume a Leontief production function with sector–level coefficients:

$$x_j(t+1) = \epsilon_j(t) \, \min\left(\min_{k \in \mathcal{S}} \frac{u_{k,j}(t)}{a_{k,j}}, \frac{\ell_j(t)}{a_{\ell,j}}, \nu_i K_i(t) \right). \tag{20}$$

Inventory dynamics. Inventories evolve according to

$$\Omega_{k,j}(t+1) = e^{-\sigma_k} \big(\Omega_{k,j}(t) + z_{k,j}(t) - u_{k,j}(t)\big), \tag{21}$$

where $\sigma_k \geq 0$ is an optional decay rate for sector k's inventories.

34

Savings and numéraire. Regional savings evolve as

$$S_r(t+1) = (1 + r_r) \max\Big\{ S_r(t) + p_{0,r}(t) \sum_{i: r(i)=r} \ell_i(t) - \sum_i p_i(t) y^c_{i,r}(t),\, 0 \Big\}, \tag{22}$$

with a region–specific interest rate r_r. To avoid nominal drifts, we normalise all prices by a wage (or a wage index) at the end of each period; for instance, we may divide all $p_i(t+1)$ and nominal stocks such as $B_r(t+1)$ and $S_r(t+1)$ by $p_{0,r^\star}(t+1)$ for a reference region $r^\star$, and reset $p_{0,r^\star}(t+1) = 1$.

8.4 Global overview of the model

$t \longleftarrow t+1$

Planning

Inputs

$x(t)$, $p(t)$, $p_0(t)$, $\Omega(t)$,

Production planning

$$\log\left(\frac{\hat{x}_i(t+1)}{x_i(t)}\right) = \beta\,\frac{\mathbb{E}_t[\Pi_i(t)]}{\mathbb{E}_t[\mathcal{G}_i(t)]+\mathbb{E}_t[\mathcal{L}_i(t)]} - \beta'\,\frac{\mathbb{E}_t[\mathcal{E}_i(t)]}{\mathbb{E}_t[\mathcal{S}_i(t)]+\mathbb{E}_t[\mathcal{D}_i(t)]},$$

Demand planning

$$z^d_{k,j}(t) = a_{k,j}\,\frac{\hat{x}_j(t+1)}{\epsilon_j(t)} + \frac{1}{\tau}\big(\hat{\Omega}_{k,j} - \Omega_{k,j}(t)\big),$$

$$\ell^d_j(t) = a_{\ell,j}\,\frac{\hat{x}_j(t+1)}{\epsilon_j(t)},$$

Demand split

$$\phi_{i|k,j} = \frac{z_{i,j}(0)}{\sum_{i':s(i')=k} z_{i',j}(0)}$$

$$z^d_{i,j}(t) = \phi_{i|k,j}\, z^d_{k,j}(t),$$

$\longrightarrow$

Exchanges

Households

$$L^d_r(t) = \sum_{i\in\mathcal{I}:r(i)=r} \ell^d_i(t)$$

$$\ell_i(t) = \ell^d_i(t)\,\min\left(1, \frac{L^s_r(t)}{L^d_r(t)}\right)$$

Transport

$$\tilde{z}^d_{i,j}(t) = \begin{cases} \chi_j(t)\chi_i(t)\, z^d_{i,j}(t) \\ \qquad \text{if } r(i) \neq r(j), \\ z^d_{i,j}(t) \\ \qquad \text{if } r(i) = r(j), \end{cases}$$

$$\tilde{y}^{q,d}_{i,r}(t) = \begin{cases} \kappa_r(t)\chi_i(t)\, y^{q,d}_{i,r}(t) \\ \text{if } i \in \mathcal{I}^{\mathrm{T}} \,\&\, r(i) \neq r, \\ y^{q,d}_{i,r}(t) \\ \qquad \text{if } r(i) = r, \end{cases}$$

Supply & Rationing

$$z_{i\to j}(t) = \lambda_i(t)\,\tilde{z}^d_{i,j}(t)$$

$$y^q_{i,r}(t) = \lambda_i(t)\phi_r(t)\,\tilde{y}^{q,d}_{i,r}(t)$$

$$q \in \{c, g\}$$

$$y_i(t) = \sum_{r\in\mathcal{R}} \big(y^c_{i,r}(t) + y^g_{i,r}(t)\big).$$

$\longrightarrow$

Capacity shock

If a climate shock happens at time t :

$$K_i(t) = (1-\zeta_i(t))K(t-1)$$

Rebuilding

If a climate shock happens at time $t-1$:

$$K_i(t) = K_i(t-1) + K^{\text{rebuild}}(t)$$

$\longrightarrow$

Production

Available quantities

$$z_{k,j}(t) := \sum_{i\in\mathcal{I}:s(i)=k} z_{i\to j}(t)$$

$$z^a_{k,j}(t) = z_{k,j}(t) + \Omega_{k,j}(t).$$

Production

$$x_j(t+1) = \epsilon_j(t)\times \min\left(\min_{k\in\mathcal{S}} \frac{u_{k,j}(t)}{a_{k,j}}, \frac{\ell_j(t)}{a_{\ell,j}}, \nu_i K_i(t)\right)$$

Inventory update

$$\Omega_{k,j}(t+1) = e^{-\sigma_k}\times \big(\Omega_{k,j}(t) + z_{k,j}(t) - u_{k,j}(t)\big)$$

Rescaling

Normalize and set $p_{0,r^\star}(t+1) = 1$

Profit & price update

$$\log\left(\frac{p_{0,r}(t+1)}{p_{0,r}(t)}\right) = \omega\,\frac{L^d_r(t) - L^s_r(t)}{L^d_r(t) + L^s_r(t)}$$

$$\log\left(\frac{p_i(t+1)}{p_i(t)}\right) = -\,\alpha\,\frac{\Pi_i(t)}{\mathcal{G}_i(t)+\mathcal{L}_i(t)} -\,\alpha'\,\frac{\mathcal{E}_i(t)}{\mathcal{S}_i(t)+\mathcal{D}_i(t)}$$

Figure 13: Summary of the model equations.